Both a hypoxia-inducible EYA3 and a histone acetyltransferase p300 function as coactivators of SIX5 to mediate tumorigenesis and cancer progression

Chunmei Yang[1], Hong Liu[2]

[1]Department of Integrated Traditional and Western Medicine, Chengdu Shangjinnanfu Hospital, Chengdu, China; [2]Department of Integrated Traditional and Western Medicine, West China Hospital of Sichuan University, Chengdu, China

Contributions: (I) Conception and design: H Liu; (II) Administrative support: H Liu; (III) Provision of study materials or patients: H Liu; (IV) Collection and assembly of data: C Yang; (V) Data analysis and interpretation: H Liu; (VI) Manuscript writing: Both authors; (VII) Final approval of manuscript: Both authors.

Correspondence to: Hong Liu. Department of Integrated Traditional and Western Medicine, West China Hospital of Sichuan University, 37 Guoxue Alley, Wuhou District, Chengdu 610041, China. Email: liuhong1980@scu.edu.cn.

Background: The transcription partners of eyes absent homologs and sine oculis homeobox homologs (EYA-SIX) contribute to tumorigenesis and progression of multiple cancers through mediating the expression of oncogenes and tumor suppressors. This study aimed to determine the roles of individual EYA-SIX partners and their downstream targets in colorectal cancer (CRC).

Methods: Immunoblot and real-time quantitative polymerase chain reaction (RT-qPCR) were used to measure protein and gene expression levels. Cell Counting Kit-8 (CCK-8) assay, colony formation, cell invasion assays, and a tumor xenograft model were chosen to investigate tumor cell growth. Immunoprecipitation, mass spectrometry, and co-immunoprecipitation (Co-IP) experiments were performed to determine the assembly of the SIX5-associated complex. Chromatin immunoprecipitation (ChIP) assay was used to evaluate the occupancy of SIX5-associated complex on its target gene promoters.

Results: We discovered that the hypoxia-induced EYA3 coupled with SIX5 and a histone acetyltransferase p300 to assemble a complex in CRC biopsies. The EYA3-SIX5-p300 complex was required for the transactivation of epidermal growth factor receptor (*EGFR*), vascular endothelial growth factor D (*VEGFD*), and five matrix metallopeptidases (*MMPs*), including *MMP3*, *MMP7*, *MMP8*, *MMP21*, and *MMP26*. The results of ChIP revealed that the EYA3-SIX5-p300 complex specifically bound to the promoters of *EGFR/VEGFD/MMPs*. Disruption of the assembly of EYA3-SIX5-p300 complex decreased the expression of *EGFR/VEGFD/MMPs*, inhibiting CRC cell growth. Administration of EYA3 inhibitor (benzarone) in mice harboring tumor xenografts significantly inhibited tumor growth.

Conclusions: The hypoxia-dependent EYA3-SIX5-p300 complex is involved in the pathogenesis of CRC through mediating *EGFR/VEGFD/MMPs* and targeting this complex may represent a new therapeutic strategy for CRC treatment.

Keywords: p300; EYA3; SIX5; colorectal cancer (CRC); epidermal growth factor receptor (EGFR)

Submitted May 10, 2022. Accepted for publication Jun 28, 2022.

doi: 10.21037/atm-22-2663

View this article at: https://dx.doi.org/10.21037/atm-22-2663

Introduction

Colorectal cancer (CRC) is the third most common cancer worldwide and the lifetime risk of developing CRC is nearly 4% in all populations (1,2). The tumorigenesis and progression of CRC arise from different causes such as genetic instability, dysregulated genes (both tumor

suppressors and oncogenes), and non-coding RNAs (microRNAs and long non-coding RNAs), the activation and inactivation of signaling pathways involved in tumorigenesis, as well as microenvironment (3,4).

Mammalian genomes encode 6 sine oculis homeobox genes (SIXs) characterized by the presence of the SIX domain (5). The SIX family proteins function as transcription factors to regulate embryogenesis by controlling the renewal and differentiation of progenitor cells (5,6). Following the complement of development, SIXs are typically downregulated (5,6). In recent years, SIX family proteins, especially SIX1, have been identified as being overexpressed in multiple cancers, such as breast cancer, ovarian cancer, prostate cancer, and CRC (7-10). Current data suggests that SIXs can regulate the expression of multiple genes involved in tumorigenesis, cell proliferation, cell migration, invasion, epithelial-to-mesenchymal transition (EMT), and metastasis (7-10). Although SIX proteins contain a DNA-binding domain, they do not harbor an intrinsic transactivation domain (6). Thus, SIXs interact with transcriptional coactivator family members called eyes absent proteins (EYAs, EYA1-4) to activate gene expression (6,7). Like SIXs, EYA members are also dysfunctional after the embryogenesis process but are overexpressed in cancers (11,12). The best demonstrated EYA-SIX partner is EYA1-SIX1, which has been identified to transactivate a series of oncogenes, such as cyclin A1 (*CCNA1*) (13), cyclin D1 (*CCND1*) (14), neuropilin 1 (*NRP1*) (15), and vascular endothelial growth factor C (*VEGFC*) (16). Except for EYAs, SIX1 can coordinate with a corepressor called dachshund homolog 1 (DACH1) to block *p53* gene expression (17).

Gene transcription is controlled by transcriptional complexes assembled by transcription factors and their regulators, such as coactivators [e.g., nuclear receptor coactivators (NOCAs), histone acetyltransferases, and lysine-specific histone demethylase 1A (KDM1A)] and corepressors [e.g., histone deacetylases (HDACs), nuclear receptor corepressors (NCOR), and C-terminal binding proteins (CtBPs)] (18-20). Although the EYA-SIX partners have been well demonstrated to control their target genes in different biological processes, it is still unknown if other transcriptional regulators also participate in the EYA-SIX-controlled transcription.

Currently, the mechanisms that upregulate SIXs and EYAs in tumorigenesis are still being investigated. The hypoxic microenvironment and the activation of hypoxia-inducible factor 1α (HIF-1α) are the two representative features of tumorigenesis and cancer progression (21). Hypoxia has been revealed to stimulate the expression of SIX1 in breast cancer cells (22). However, whether hypoxia induces EYA-SIX partners is still unclear in CRC cells.

Although many studies have discovered that numerous dysregulated signalings and genes may contribute to CRC pathogenesis (3,4), the functions of the EYA-SIX partners and their target genes in CRC tumorigenesis are still obscure. Recently, we explored the expression patterns of six SIX members and four EYA members in cancerous CRC biopsies and CRC cells, and we found that SIX1 and three EYAs (EYA1, EYA3, and EYA4) were upregulated (10). We revealed that the EYA1-SIX1 partner controlled the expression of *CCNA1* and transforming growth factor-beta 1 (*TGFB1*) in the pathogenesis of CRC (10). However, it is still unclear how EYA3 and EYA4 couple with other transcription factors to contribute to CRC tumorigenesis and progression. In the present study, we focused our investigation on revealing the EYA3-associated complex and its downstream target genes in CRC. Our results demonstrated that the hypoxia-induced EYA3 assembled a transcriptional complex with SIX5 and a histone acetyltransferase p300. This complex transactivated the expression of epidermal growth factor receptor (*EGFR*), vascular endothelial growth factor D (*VEGFD*), and five matrix metallopeptidases (*MMPs*) genes by binding to their promoters. Dysfunction of the EYA3-SIX5-p300 complex inhibited the expression of *EGFR/VEGFD/MMPs*. Our findings reveal the mechanism of how the EYA3-SIX5-p300 complex contributes to CRC pathogenesis and provide a new therapeutic strategy to inhibit CRC cell growth. We present the following article in accordance with the ARRIVE reporting checklist (available at https://atm.amegroups.com/article/view/10.21037/atm-22-2663/rc).

Methods

Cell culture and transfection

Seven CRC cell lines (HT-29, HT55, HCT-15, HCT-116, HCA-24, SW620, and T84) and one noncancerous human colon epithelial cell line (HCEC-1CT) were acquired from the American Type Culture Collection (ATCC; Manassas, VA, USA). Cells were cultured in Dulbecco's modified Eagle's medium (DMEM; Corning, Shanghai, China; #10013CV) containing 10% (v/v) fetal bovine serum (FBS; Corning; #35010CV) at 37 ℃ in a 5% CO_2 incubator. Cells under 90% confluence were transfected with plasmids

(Table S1) or two independent short hairpin RNAs (shRNAs) targeting each gene (Table S2) following a previous protocol (10).

Tumor xenograft model in mouse

We purchased BALB/c mice from Beijing Vital River Laboratories (Beijing, China) and maintained them in a specific-pathogen-free (SPF) facility with a 12-hour light/dark cycle and free access to water and food. Cells (1×10^6) were suspended in 100 µL of phosphate-buffered saline (PBS) and then implanted into the right flank of 10-week-old mice (female, weight: 22–24 g, n=10 for each cell line). Tumor volumes were measured every five days. Tumor volumes were determined using the formula: tumor volume = (length × width^2)/2. To evaluate the inhibitory effect of the EYA3 inhibitor benzarone (Sigma-Aldrich, Shanghai, China; #B0490000), HT-29 cells (1×10^6) were injected into the right flank of 10-week-old mice (female, weight: 22–24 g, n=40). After tumor volumes had reached approximately 150 mm^3, mice were randomly divided into four subgroups, which were intravenously injected with PBS (control), 50, 100, and 200 mg/kg benzarone (n=10 for each subgroup) at a five-day interval, respectively. At the end of the experiment, mice were sacrificed, and tumors were collected. All mice were grown in the same SPF room. The first author was aware of the group allocation during the experiments. Animal experiments were performed under a project license (No. 2018072HA) granted by the ethics board of West China Hospital of Sichuan University, in compliance with guidelines for the care and use of animals at West China Hospital of Sichuan University.

Data analysis from The Cancer Genome Atlas (TCGA)

Gene expression data and clinical information of 104 CRC patients (50 patients expressed higher levels of EYA3 and 54 patients expressed lower levels of EYA3) were downloaded from TCGA database (https://portal.gdc.cancer.gov/). Approximately 45.2% CRC patients were male and the other 54.8% patients were female. Ages of CRC patients ranged from 47 to 81 years with a median age of 64.3 years. Kaplan-Meier survival curves were used to determine the effects of EYA3 expression levels on overall survival abilities. The study was conducted in accordance with the Declaration of Helsinki (as revised in 2013).

Cell viability and invasion assays

For cell viability, cells were seeded into 96-well plates at a density of nearly 2,500 cells/well. Cell proliferation was determined at different time points (days 0, 1, 2, 3, 4, and 5) using the Cell Counting Kit-8 (CCK-8; Sigma-Aldrich; #96992) according to the guidelines provided by the manufacturer. For cell invasion, nearly 1×10^5 cells were seeded into the upper chambers of a CultreCoat BME Cell invasion assay kit (R&D systems, Shanghai, China; #3481096K) and incubated at 37 ℃ for 24 hours. The invaded cells in the lower chambers were fixed with methanol and stained with 0.1% (w/v) crystal violet (Sigma-Aldrich; #C6158).

Immunoprecipitation and mass spectrometry

Equal weights of three independent cancerous biopsies were mixed and lysed in a radioimmunoprecipitation assay (RIPA) buffer (Sigma-Aldrich; #R0278) supplemented with a protease inhibitor cocktail (Sigma-Aldrich; #11697498001) for 30 minutes at 4 ℃. Cell lysates were centrifuged at 13,000 rpm for 15 minutes at 4 ℃. The soluble fraction was immunoprecipitated with anti-EYA3 (Proteintech, Wuhan, Hubei, China; #21196-1-AP) associated protein A agarose (Abcam, Shanghai, China; #ab193255). The immunoprecipitates were rinsed six times with RIPA buffer, followed by denaturation in the sodium dodecyl sulfate (SDS) loading buffer. The denatured samples were loaded onto a 10% SDS-polyacrylamide gel electrophoresis (PAGE) gel, followed by silver staining with a kit (Thermo Fisher, Shanghai, China; #24612). The visualized protein bands were destained and digested with sequencing grade trypsin (Thermo Fisher; #90057) overnight at 37 ℃. The eluted peptides were analyzed using a mass spectrometer (Thermo Fisher; #TSQ02-21002) and the obtained data were searched in an in-house Mascot server (Matrix Science, London, UK) against the international protein index with a significance threshold (<0.05).

RNA extraction and quantitative real-time polymerase chain reaction

Total RNA was extracted from cells and biopsies using TRIzol reagent (Thermo Fisher; #15596026). For each sample, 1 µg of total RNA was reverse-transcribed into complementary DNA (cDNA) using the M-MuLV reverse

transcriptase (New England Biolabs, Shanghai, China; #M0253S). After dilution for 10-fold, 1 μL cDNA in each sample was used as the template to perform quantitative real-time polymerase chain reaction (qRT-PCR) with the SYBR Green Supermix (Bio-Rad Laboratories, Shanghai, China; #1725270). The primers are all listed in Table S3. The relative messenger RNA (mRNA) level of an individual gene was determined using the $2^{-\Delta\Delta CT}$ method by normalizing it to Actin.

Western blot assay

Total proteins were extracted using RIPA buffer containing a protease inhibitor cocktail. After centrifuging at 13,000 rpm for 15 minutes at 4 ℃, the soluble cell extracts were used for immunoblots according to a previous protocol (10). The primary antibodies included the following: anti-EYA3 (Proteintech, Wuhan, Hubei, China; #21196-1-AP), anti-SIX5 (Invitrogen, Shanghai, China; #PA5-75417), anti-p300 (Santa Cruz Biotechnology, Shanghai, China; sc-48343), anti-GAPDH (Santa Cruz Biotechnology; #sc-47724), anti-Flag (Sigma-Aldrich; #SAB4200071), and anti-Myc (Invitrogen; #R95125). The horseradish peroxidase (HRP)-conjugated secondary antibodies included the following: anti-mouse immunoglobulin G (IgG) (Sigma-Aldrich; #GENA931) and HRP-conjugated anti-rabbit IgG (Sigma-Aldrich; #GENA934).

Immunohistochemistry (IHC) assay

The IHC assay was performed following a previous method (10). The tissue slices were stained using anti-EYA3. Slides were imaged using an inverted TE 2000 wide-field microscope (Nikon, Tokyo, Japan).

Co-immunoprecipitation (Co-IP) assay

Cells expressing different combinations of plasmids were lysed in RIPA buffer plus 1% protease inhibitor cocktail at 4 ℃ for 2 hours. After centrifuging at 13,000 rpm for 15 minutes at 4 ℃, the supernatant was immunoprecipitated using anti-Flag antibody-conjugated Sepharose beads (Abcam, Shanghai, China; #ab270704) and anti-Myc antibody conjugated Sepharose beads (Sigma-Aldrich; #A7470), respectively. After incubation at 4 ℃ for 2 hours, the beads were rinsed five times with RIPA buffer, followed by boiling with SDS loading buffer and separating in 10% SDS-PAGE gels. The input and output proteins were probed using anti-Myc and anti-Flag.

Chromatin immunoprecipitation (ChIP) assay

Cells were fixed with 1% (w/v) formaldehyde (Sigma-Aldrich; #433284) for 15 minutes, quenched with 125 mM glycine (Sigma-Aldrich; #G8898) for 5 minutes, and washed three times with PBS buffer. Cells were then lysed in the ChIP lysis buffer containing 50 mM HEPES/KOH (pH 7.5), 75 mM NaCl, 1 mM ethylenediamine tetraacetic acid (EDTA), 1% Triton X-100, 0.1% SDS, and 1% protease inhibitor cocktail. Cell lysates were sonicated to reach a 500 bp length of average size, followed by an assay with a ChIP kit (Abcam; #ab500). The input and output DNA were subjected to qRT-PCR analyses to measure the occupancies of EYA3-associated transcriptional complex members on the promoters of genes with the primers listed in Table S4.

Statistical analysis

All experiments were independently repeated in triplicate. Data were presented as the mean ± standard deviation (SD). Statistical analysis was performed using SPSS 19.0 software (IBM Corp., Chicago, IL, USA). The differences between the two groups were analyzed using a Student's *t*-test. Figures were generated using GraphPad Prism 8 software (GraphPad Inc., San Diego, CA, USA). Statistical significance was set at a P value less than 0.05.

Results

EYA3 was overexpressed in CRC biopsies and cells

We previously detected the expression patterns of SIXs and EYAs in 24-paired biopsies from CRC patients and discovered that SIX1 and three EYAs (EYA1, EYA3, and EYA4) were upregulated in the cancerous biopsies compared to their adjacent noncancerous tissues (10). We have revealed the functions of EYA1-SIX1 partners in the regulation of genes involved in CRC tumorigenesis. We next aimed to investigate the role of EYA3 and its transcriptional partners. Using the new 20 pairs of biopsies collected from CRC patients, we detected the mRNA levels of *EYA3* and we also observed the induction (nearly 2.62±0.33-fold) of *EYA3* in the cancerous tissues in comparison to the controls (*Figure 1A*). Consistently, we also observed the elevation of EYA3 protein levels in

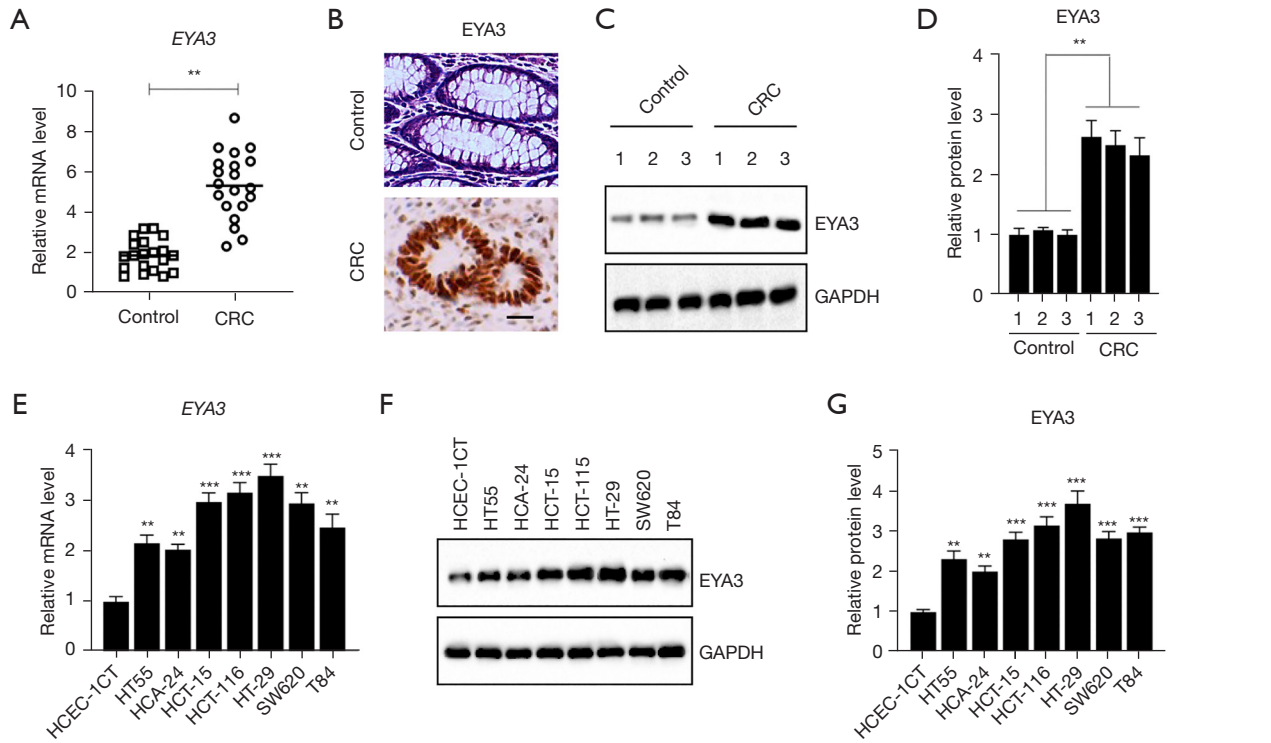

Figure 1 EYA3 was elevated in the CRC cancerous biopsies and CRC cells. (A) *EYA3* mRNA levels in cancerous CRC biopsies and their adjacent noncancerous tissues (Control) (n=20). **, P<0.01. (B) IHC staining results of EYA3 in one representative group of cancerous CRC biopsy and its adjacent noncancerous tissue. Bars =100 μm. (C,D) EYA3 protein levels in three representative groups of cancerous CRC biopsies and their adjacent noncancerous tissues. GAPDH was used as the loading control. (C) Immunoblot result. (D) Quantified protein levels. **, P<0.01. (E) *EYA3* mRNA levels in HCEC-1CT cells and seven CRC cell lines (HT55, HCA-24, HCT-15, HCT-116, HT-29, SW620, and T84). **, P<0.01 and ***, P<0.001. (F,G) EYA3 protein levels in CRC cells. GAPDH was used as the loading control. (F) Immunoblot result. (G) Quantified protein levels (comparing with HCEC-1CT). **, P<0.01 and ***, P<0.001. mRNA, messenger RNA; CRC, colorectal cancer; IHC, immunohistochemistry.

the cancerous tissues using IHC and immunoblot assays (*Figure 1B-1D*).

Using one noncancerous cell line HCEC-1CT as a control, we also measured the mRNA and protein levels of EYA3 in seven CRC cell lines (HT-29, HT55, HCT-15, HCT-116, HCA-24, SW620, and T84). Both the real-time quantitative polymerase chain reaction (RT-qPCR) and immunoblot results showed that *EYA3* mRNA and protein levels were upregulated in CRC cell lines compared to that in the HCEC-1CT cell line (*Figure 1E-1G*). Of these seven CRC cells, *EYA3* mRNA and protein levels were mostly increased in HT-29 cells (nearly 3.34±0.41-fold, P<0.001) but such increases were the lowest in the HCA-24 cells (nearly 1.91±0.22-fold, P<0.01) (*Figure 1E-1G*).

EYA3 was induced by hypoxia in vitro

Given that hypoxia is a common feature in tumorigenesis and cancer progression, we next aimed to evaluate if the two hypoxia response transcription factors HIF-1α and HIF-2α were elevated in CRC biopsies. The immunoblot results indicated that both HIF-1α and HIF-2α were increased (HIF-1α 3.14±0.39-fold; HIF-α 2.07±0.26-fold) in three representative pairs of cancerous biopsies compared to their adjacent noncancerous controls (*Figure 2A,2B*). Using hypoxia-treated HCEC-1CT cells at different time points (0, 3, 6, and 9 h), we found that HIF-1α, HIF-2α, and EYA3 protein levels all gradually increased in a time-dependent manner and they showed similar expression patterns (*Figure 2C,2D*).

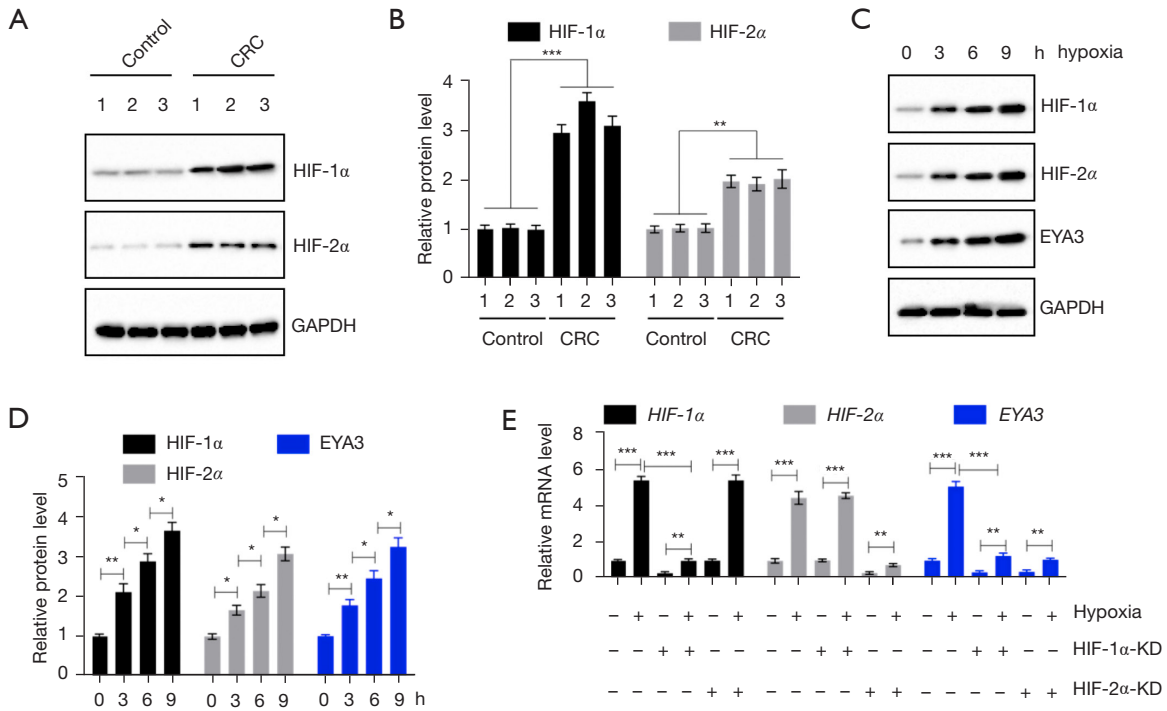

Figure 2 Hypoxia induced the expression of EYA3. (A,B) Protein levels of HIF-1α and HIF-2α in three representative groups of cancerous CRC biopsies and their adjacent noncancerous tissues. GAPDH was used as the loading control. (A) Immunoblot result. (B) Quantified protein levels. **, P<0.01 and ***, P<0.001. (C,D) Protein levels of HIF-1α, HIF-2α, and EYA3 in hypoxia-treated cells (treatment with hypoxia for 0, 3, 6, and 9 h). GAPDH was used as the loading control. (C) Immunoblot result. (D) Quantified protein levels. *, P<0.05 and **, P<0.01. (E) The mRNA levels of *HIF-1α*, *HIF-2α*, and *EYA3* in the Control-KD, HIF-1α-KD, and HIF-2α-KD cells treated with or without hypoxia for 9 h. **, P<0.01 and ***, P<0.001. mRNA, messenger RNA; HIF-1α, hypoxia-inducible factor 1α; CRC, colorectal cancer; HIF-1α, hypoxia-inducible factor 1α; KD, knockdown.

We next evaluated if the expression level of *EYA3* was dependent on HIF-1α and HIF-2α. For this purpose, we generated the knockdown (KD) cell lines of both HIF-1α and HIF-2α and then treated cells with or without hypoxia for 9 hours. Hypoxia significantly induced *HIF1α*, *HIF2α*, and *EYA3* mRNA levels (*Figure 2E*). Following the depletion of HIF-1α and HIF-2α *EYA3* mRNA level was also decreased, and hypoxia treatment only induced the *EYA3* mRNA level in HIF-1α-KD and HIF-2α-KD cells to a level comparable to that in non-treated HCEC-1CT cells (*Figure 2E*). These results revealed that the induction of EYA3 in CRC biopsies and cells was dependent on hypoxia and HIF transcription factors.

The deficiency of EYA3 in CRC cells decreased cell proliferation and invasion

To explore the clinical significance of *EYA3*, we analyzed the expression level of *EYA3* in the clinical dataset of CRC patient samples collected from the TCGA database. The Kaplan-Meier survival curves indicated that the higher expression level of *EYA3* was associated with a worse overall survival (OS) rate (*Figure 3A*).

Using HT-29 cells, we generated two independent control-KD cell lines and two EYA3-KD cell lines (*Figure 3B*). Cell proliferation and invasion assays showed that the deficiency of *EYA3* significantly decreased cell viability and invasion rate (*Figure 3C,3D*, and Figure S1). Similarly, we also created two independent control-KD cell lines and two EYA3-KD cell lines in the HCA-24 background (*Figure 3E*). We also observed the similar effects of EYA3 depletion on cell proliferation and invasion (*Figure 3F,3G*, and Figure S1).

EYA3 assembled a transcriptional complex with SIX5 and a histone acetyltransferase p300

To dissect the EYA3-associated transcriptional complex members, we purified the EYA3-associated complex in

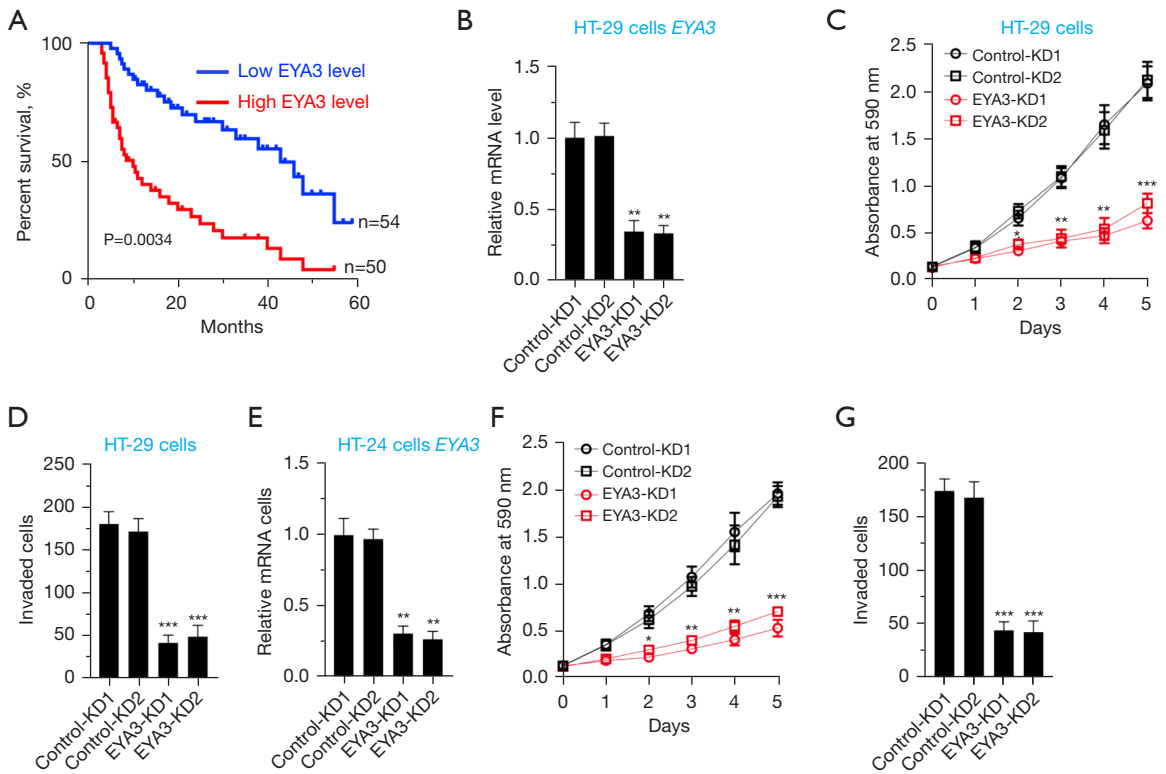

Figure 3 Knockdown of EYA3 inhibited cell proliferation and invasion. (A) Kaplan-Meier survival curves. Data were collected from TCGA database. Red line: higher expression level of *EYA3*; blue line: lower expression level of *EYA3*. (B) *EYA3* mRNA levels in control-KD and EYA3-KD cells under HT-29 background. **, P<0.01. (C) Cell viability of control-KD and EYA3-KD cells (HT-29 background) at different time points (0, 1, 2, 3, 4, and 5 days). *, P<0.05; **, P<0.01; and ***, P<0.001. (D) Invaded cell numbers of Control-KD and EYA3-KD cells (HT-29 background). ***, P<0.001. (E) *EYA3* mRNA levels in Control-KD and EYA3-KD cells under HCA-24 background. **, P<0.01. (F) Cell viability of control-KD and EYA3-KD cells (HCA-24 background) at different time points (days 0, 1, 2, 3, 4, and 5). *, P<0.05; **, P<0.01; and ***, P<0.001. (G) Invaded cell numbers of control-KD and EYA3-KD cells (HCA-24 background). ***, P<0.001. TCGA, The Cancer Genome Atlas; KD, knockdown.

CRC biopsies using anti-EYA3-conjugated agarose. Mass spectrometry identified 62 EYA3-interacting proteins (Table S5), which included a transcription factor SIX5 and a transcriptional regulator p300 (Table S5). Using the mixture of another three CRC biopsies, we performed an immunoprecipitation assay with anti-EYA3-conjugated agarose, which revealed that SIX5 and p300 could also be pulled down by EYA3 (*Figure 4A*). To further solidify that EYA3 assembled a complex, we expressed pCDNA3-Flag-EYA3 in HCEC-1CT cells and then conducted an immunoprecipitation assay using anti-Flag-agarose. The results also indicated that EYA3 could pull down both SIX5 and p300 *in vitro* (*Figure 4B*).

To determine how EYA3 assembled a complex with SIX and p300, we performed Co-IP assays to evaluate the direct interaction between EYA3-p300, EYA3-SIX5, and SIX5-p300. The immunoblot results demonstrated that EYA3 could directly interact with SIX5 but not p300, and SIX5 could directly interact with both EYA3 and p300 (*Figure 4C*,*4D*). These results suggested that SIX5 recruited both p300 and EYA3 to form a transcriptional complex (*Figure 4E*).

Hypoxia promoted the assembly of the EYA3-SIX5-p300 complex

We next evaluated if hypoxia treatment could affect the assembly of the EYA3-SIX5-p300 complex. For this purpose, we treated HCEC-1CT cells with hypoxia for different durations (0, 3, 6, and 9 h), followed by

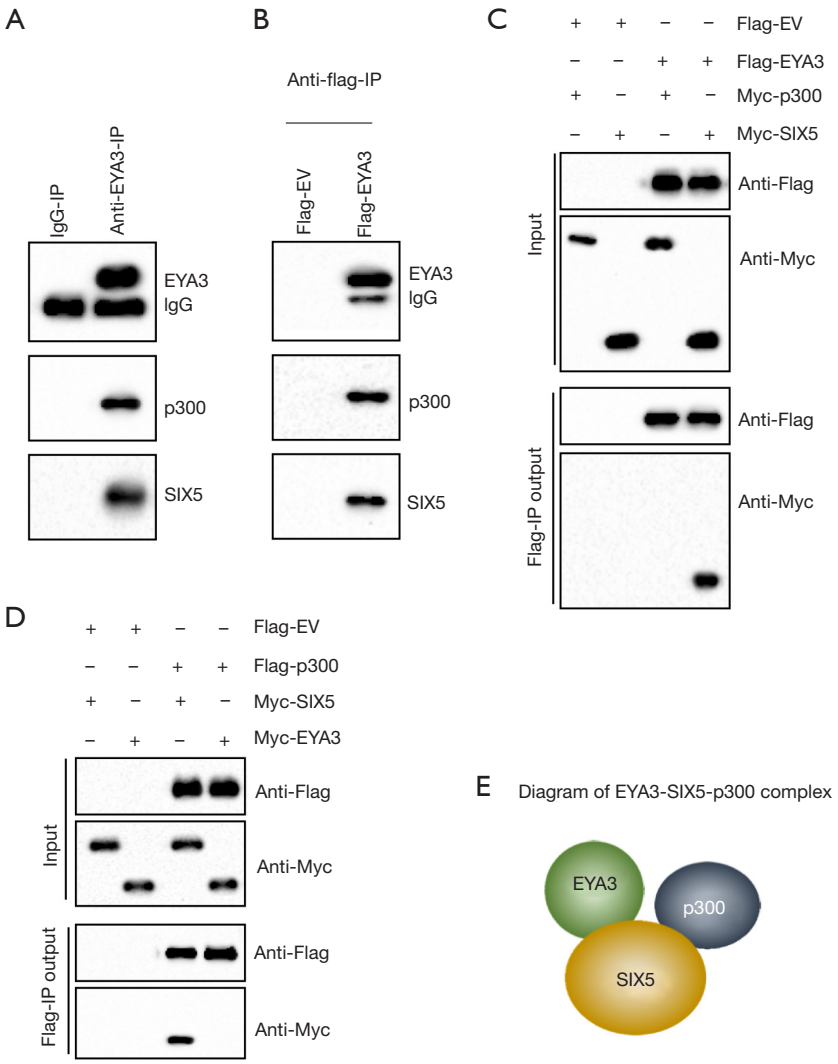

Figure 4 The assembly of EYA3-SIX5-p300 complex *in vivo* and *in vitro*. (A) EYA3 pulled down both SIX5 and p300 in cancerous biopsies. Three independent cancerous were mixed with equal weights and were then immunoprecipitated using anti-EYA3 (or IgG, negative control) conjugated agarose. The output complexes were probed with antibodies as indicated in the figure. (B) EYA3 pulled down both SIX5 and p300 in HCEC-1CT cells expressing pCDNA3-Flag-EYA3. (C,D) Detection of direct interaction of EYA3-p300, EYA3-SIX5, p300-SIX5, and p300-EYA3 *in vitro*. Different combinations of plasmids as shown in the figure were transfected into HCEC-1CT cells, followed by immunoprecipitation with anti-Flag- and anti-Myc-agarose. The outputs were probed using anti-Flag and anti-Myc. (C) Interactions of EYA3-p300 and EYA3-SIX5. (D) Interactions of p300-SIX5 and p300-EYA3. (E) Schematic assembly of the EYA3-SIX5-p300 complex. IgG, immunoglobulin G.

immunoprecipitation using anti-EYA3-conjugated agarose. Consistent with the observation in *Figure 2C*, the immunoprecipitated EYA3 was gradually increased following the prolongation of hypoxia treatments (Figure S2A). Meanwhile, we found the immunoprecipitated SIX5 and p300 by EYA3 also showed similar patterns to EYA3 (Figure S2A).

Using hypoxia-treated HIF-1α-KD and HIF-2α-KD cells, we performed immunoprecipitation using anti-EYA3-conjugated agarose. The results also indicated that the immunoprecipitated EYA3 in HIF-1α/2α-KD cells and hypoxia-treated HIF-1α/2α-cells were much less than that in the control-KD and hypoxia-treated control-KD cells, respectively (Figure S2B). Similarly, the immunoprecipitated

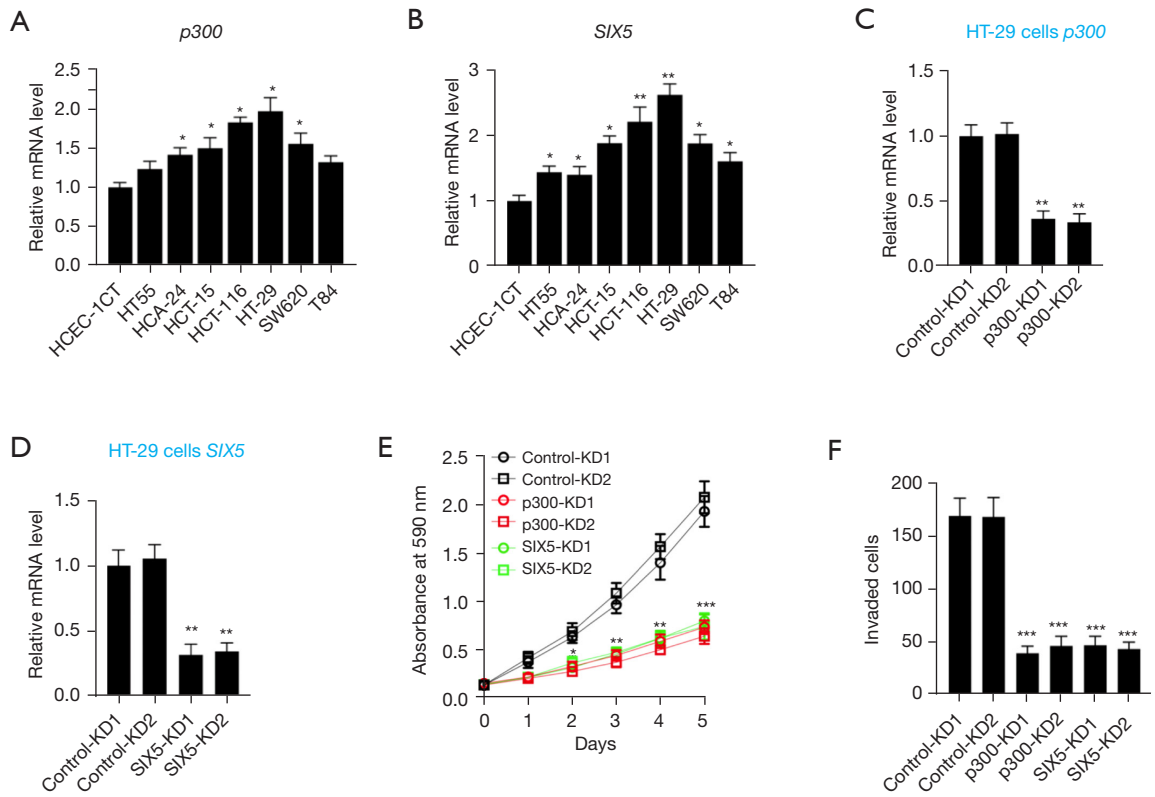

Figure 5 Knockdown of SIX5 and p300 inhibited cell proliferation and invasion. (A,B) *p300* and *SIX5* mRNA levels in HCEC-1CT cells and seven CRC cell lines (HT55, HCA-24, HCT-15, HCT-116, HT-29, SW620, and T84). *, P<0.05 and **, P<0.01. (A) p300; (B) SIX5. (C) *p300* mRNA levels in control-KD and p300-KD cells under HT-29 background. **, P<0.01. (D) SIX5 mRNA levels in control-KD and SIX5-KD cells under HT-29 background. **, P<0.01. (E) Cell viability of Control-KD, p300-KD, and SIX5-KD cells (HT-29 background) at different time points (days 0, 1, 2, 3, 4, and 5). *, P<0.05; **, P<0.01; and ***, P<0.001. (F) Invaded cell numbers of control-KD, p300-KD, and SIX5-KD cells (HT-29 background). ***, P<0.001. CRC, colorectal cancer; KD, knockdown.

SIX5 and p300 by EYA3 also showed similar patterns to EYA3 in all cells (Figure S2B). These results suggested that hypoxia promoted the assembly of the EYA3-SIX5-p300 complex.

Deficiency of p300 and SIX5 in CRC cells decreased cell proliferation, invasion, and tumor growth

Since EYA3 was elevated in CRC cells, we next measured the expression levels of p300 and SIX5. Using the same seven CRC cell lines and HCEC-1CT control, we found that the *p300* mRNA level was slightly increased (from 1.32- to 2.04-fold) in five cell lines (HCA-24, HCT-15, HCT-116, HT-29, and SW620) and the *SIX5* mRNA level was similar to the pattern of EYA3 (*Figure 5A*,*5B*). We next generated two independent p300-KD and SIX5-KD cell lines in the HT-29 background (*Figure 5C*,*5D*). Using these cells, we performed cell proliferation and invasion experiments and the results showed that the depletion of either p300 or SIX5 caused cell growth inhibition and suppressed cell invasion (*Figure 5E*,*5F*, and Figure S3). In addition, we also injected control-KD, EYA3-KD, p300-KD, and SIX5-KD cells into mice to generate tumors and then measured tumor volumes at a 5-day interval. The tumor volumes in mice harboring EYA3-KD, p300-KD, and SIX5-KD cells were much smaller than those in mice injected with control-KD cells (Figure S4). Tumor volumes were not obviously different among mice injected with

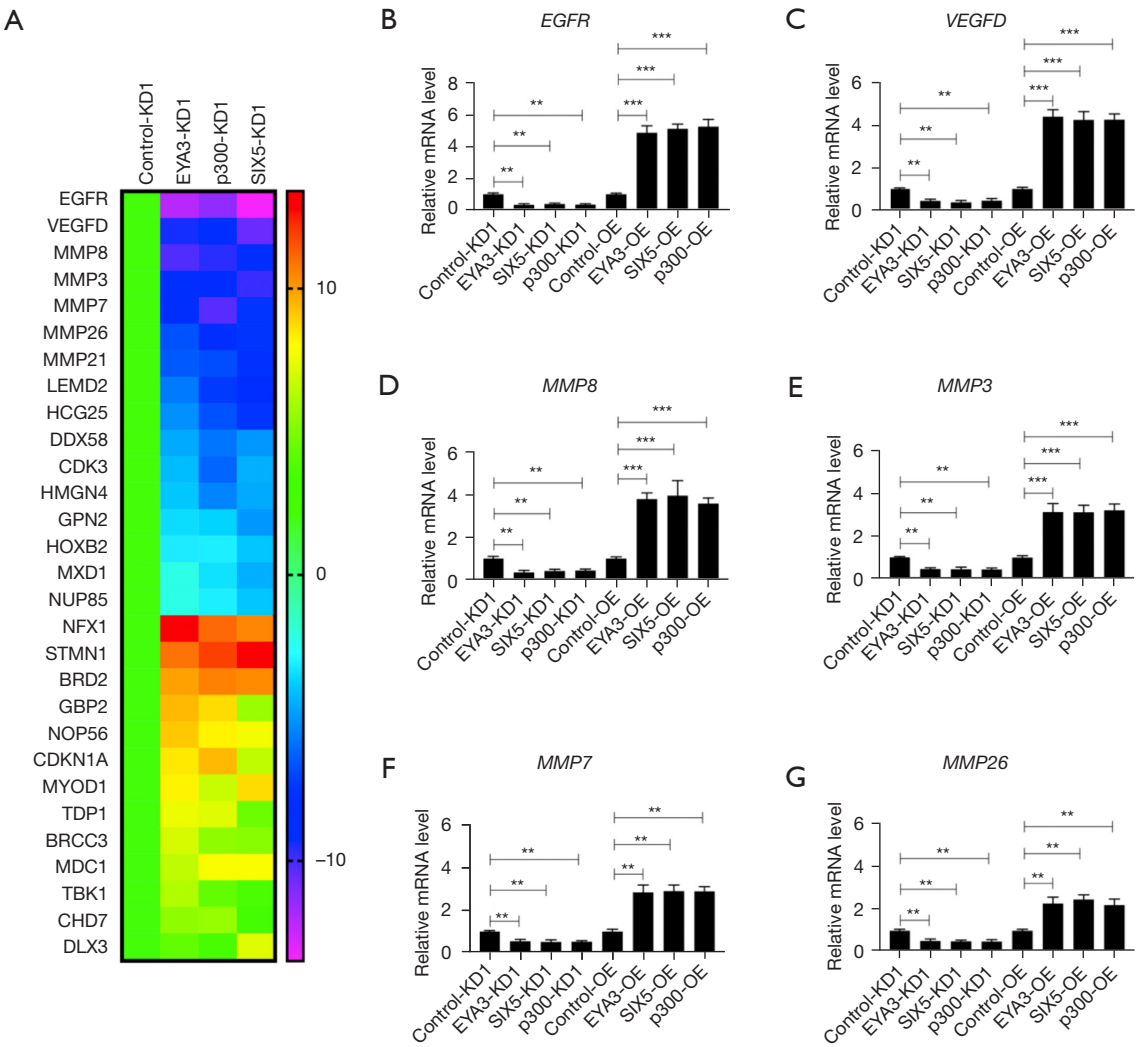

Figure 6 Identification of dysregulated genes that were dependent on EYA3-SIX5-p300 complex and verification of their expression levels. (A) Heatmap of microarray results in control-KD1, EYA3-KD1, p300-KD1, and SIX5-KD1 cells. (B-G) The mRNA levels of *EGFR* (B), *VEGFD* (C), *MMP8* (D), *MMP3* (E), *MMP7* (F), and *MMP26* (G) in the KD and OE cell lines of EYA3, p300, and SIX5. **, P<0.01, and ***, P<0.001. KD, knockdown; OE, overexpression; EGFR, epidermal growth factor receptor; VEGFD, vascular endothelial growth factor receptor; MMP, matrix metalloproteinase.

EYA3-KD, p300-KD, and SIX5-KD cells (Figure S4).

The EYA3-SIX5-p300 complex was required for the transregulation of multiple genes involved in tumorigenesis and cancer progression

To identify the downstream target genes of the EYA3-SIX5-p300 complex, we performed a microarray analysis using control-KD1, EYA3-KD1, p300-KD1, and SIX5-KD cells. After analyzing the overlapped genes that were dysregulated in EYA3-KD1, p300-KD1, and SIX5-KD cells compared to the control-KD1 cells, we discovered 29 genes, which included 16 downregulated genes and 13 upregulated genes (Table S6 and *Figure 6A*). Among them, we observed epidermal growth factor receptor (*EGFR*), vascular endothelial growth factor D (*VEGFD*), and five matrix metallopeptidases (*MMPs*; including *MMP3*, *MMP7*, *MMP8*, *MMP21*, and *MMP26*) (Table S6 and *Figure 6A*). These genes have been previously shown to participate in tumorigenesis and cancer progression.

To determine if the microarray data were reliable, we selected 10 representative genes [*EGFR*, *VEGFD*, *MMP3*, *MMP7*, *MMP8*, *MMP26*, *RNF5* (ring finger protein 5), *TAP2* (transporter 2), *STMN1* (stathmin 1), and *BRD2* (bromodomain containing 2)] and measured their expression levels in the KD (HT-29 background) and overexpression (OE; HCEC-1CT background) cell lines of EYA3-SIX5-p300 members. Consistent with the microarray results, we observed that the downregulation of *EGFR*, *VEGFD*, *MMP3*, *MMP7*, *MMP8*, *MMP26*, and *RNF5* was decreased in the EYA3-KD1, p300-KD1, and SIX5-KD cells compared to the control-KD1 cells (*Figure 6B-6G* and Figure S5A). In contrast, these seven genes were upregulated in the OE cell lines (*Figure 6B-6G* and Figure S5A). The other three genes (*TAP2*, *STMN1*, and *BRD2*) were upregulated in the KD cells but downregulated in the OE cells of EYA3-SIX5-p300 members (Figure S5B-S5D).

Given the importance of *EGFR*, *VEGFD*, *MMP3*, *MMP7*, *MMP8*, and *MMP26* in tumorigenesis and cancer progression, we next measured their expression levels in 20-pairs of CRC biopsies and their adjacent noncancerous tissues. Our results indicated that these genes were all elevated in the cancerous tissues (Figure S6A-S6F).

The EYA3-SIX5-p300 complex controlled the expression of EGFR/VEGFD/MMPs through binding to their promoters

To determine if *EGFR*, *VEGFD*, *MMP3*, *MMP7*, *MMP8*, *MMP21*, and *MMP26* were the direct targets of the EYA3-SIX5-p300 complex, we analyzed the promoters (2,000 bp length) of these seven genes to identify the SIX5 binding sites using the TCA(A/G)(A/G)TTNC (N represents any nucleotide) consensus sequence. We found that each of these gene promoters contained a SIX5 binding site (*Figure 7A*). We then performed ChIP assays in the KD and OE cell lines of EYA3-SIX5-p300 members (the same as that used in *Figure 6*) using anti-EYA3, anti-SIX5, anti-p300, and IgG (negative control). The results indicated that the enrichment of EYA3, SIX5, and p300 on the promoters of *EGFR*, *VEGFD*, *MMP3*, *MMP7*, *MMP8*, *MMP21*, and *MMP26* were all decreased in the KD cell lines but increased in the OE cell lines compared to the controls (*Figure 7B-7D* and Figure S7). Meanwhile, we also detected the expression of *MMP13* (its promoter does not contain a SIX5 binding site) in the KD and OE cell lines of EYA3-SIX5-p300 members. We found that the depletion or OE of EYA3-SIX5-p300 members could not change the expression of *MMP13* (Figure S8A). The ChIP assay results also supported that the EYA3-SIX5-p300 complex could not bind to the promoter of *MMP13* (Figure S8B). These results suggested that *EGFR*, *VEGFD*, *MMP3*, *MMP7*, *MMP8*, *MMP21*, and *MMP26* instead of *MMP13* were the direct targets of the EYA3-SIX5-p300 complex.

An EYA3 inhibitor benzarone could block the assembly of the EYA3-SIX5-p300 complex and inhibited CRC growth in vitro and in vivo

The results in *Figures 3*,*5* suggested that the EYA3-SIX5-p300 complex might be a potential therapeutic target for CRC treatment. To demonstrate this hypothesis, we treated HT-29 cells with different doses (0, 10, 20, and 30 μM) of an EYA3 inhibitor called benzarone (*Figure 8A*), followed by an immunoprecipitation assay with anti-EYA3-conjugated agarose. We found that the immunoprecipitated p300 and SIX5 by EYA3 were dose-dependently decreased following benzarone treatments (*Figure 8B*). Meanwhile, benzarone treatments also caused the dose-dependent suppression of *EGFR*, *VEGFD*, *MMP3*, *MMP7*, *MMP8*, and *MMP26* (*Figure 8C-8H*). The ChIP assay results revealed that benzarone treatments caused the dose-dependent decrease in the enrichment of EYA3-SIX5-p300 members on the promoters of *EGFR*, *VEGFD*, *MMP3*, *MMP7*, *MMP8*, *MMP21*, and *MMP26* (*Figures S9*,*S10*). Consistent with the observation in cells depleted EYA3-SIX5-p300 members, we also found that benzarone treatments resulted in a dose-dependent deduction of cell proliferation (Figure S11A), cell invasion (Figure S11B,S11C), and tumor growth *in vivo* (Figure S11D).

Discussion

The *EYA3* gene functions as a transcriptional partner of SIX transcription factors and the elevation of its expression level has been observed in multiple tumors (11,12). However, three main questions, including the underlying mechanism of EYA3 upregulation, the components of EYA3-associated complex, and the downstream target genes regulated by EYA3-associated complex in the genome-wide, had remained unanswered until now. In the current study, we found that hypoxia induced the expression of *EYA3* and promoted the assembly of EYA3-SIX5-p300 in CRC cells. The EYA3-SIX5-p300 complex bound to the promoters of *EGFR*, *VEGFD*, *MMP3*, *MMP7*, *MMP8*, *MMP21*, and *MMP26* and induced their expression, thus causing tumorigenesis and promoting cancer progression

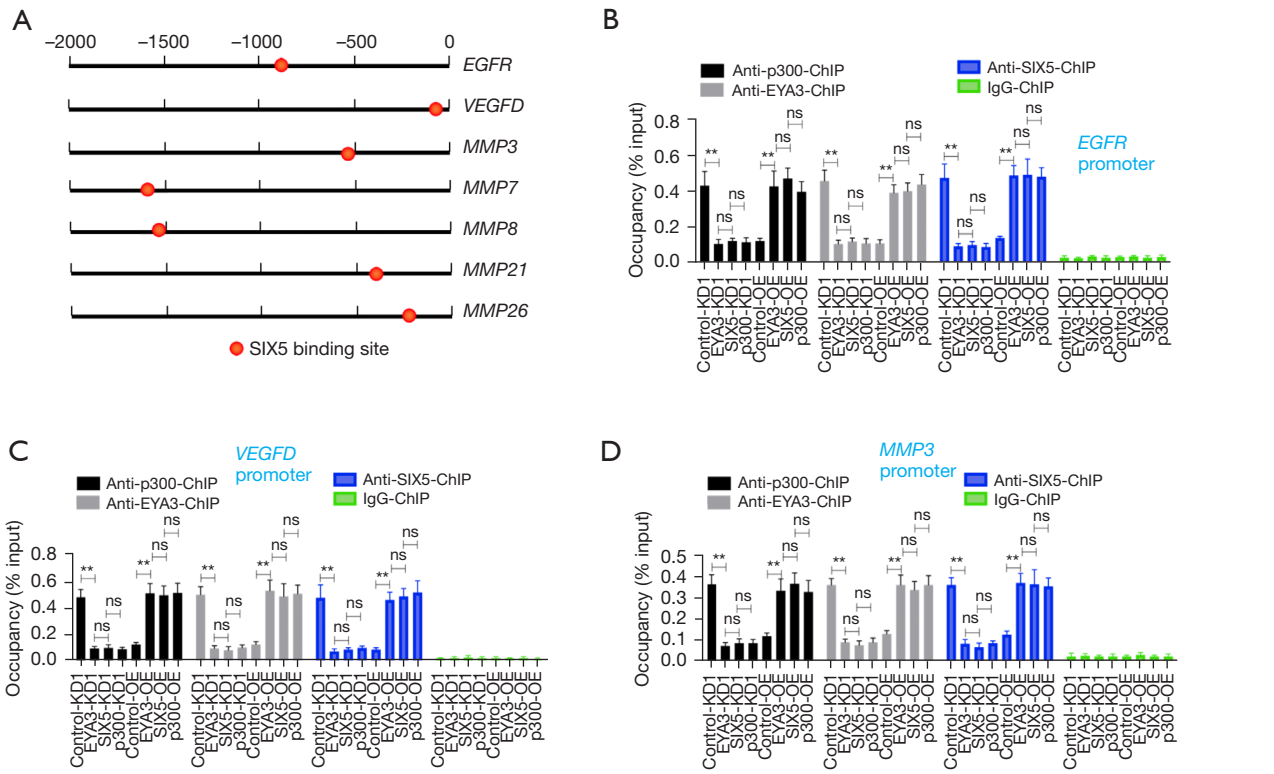

Figure 7 The EYA3-p300-SIX5 members bound to the promoters of *EGFR*, *VEGFD*, and *MMP3*. (A) Diagrams of the SIX5 binding site on the promoters (2,000 bp length) of *EGFR*, *VEGFD*, *MMP8*, *MMP3*, *MMP7*, MMP21, and *MMP26*. (B-D) Occupancies of EYA3-p300-SIX5 members on the promoters of *EGFR* (B), *VEGFD* (C), and *MMP3* (D). Different cells as indicated in the figure were used for ChIP assays with anti-EYA3, anti-p300, anti-SIX5, and IgG (negative control). The input and output DNA were subjected to qRT-PCR analyses to measure the enrichment of EYA3-p300-SIX5 members on the promoters of *EGFR*, *VEGFD*, and *MMP3*. **, P<0.01. ns, no significant difference; KD, knockdown; OE, overexpression; EGFR, epidermal growth factor receptor; VEGFD, vascular endothelial growth factor receptor; MMP, matrix metalloproteinase; ChIP, chromatin immunoprecipitation; qRT-PCR, quantitative real-time polymerase chain reaction.

(*Figure 9A*). The depletion of EYA3-SIX5-p300 members or the blockage of EYA3-SIX5-p300 assembly by an EYA3 inhibitor benzarone can impair the expression of the downstream target genes, inhibiting CRC cell growth *in vitro* and *in vivo* (*Figure 9B*).

The EYA family proteins function as both transcriptional coactivators and tyrosine phosphatases (11,12). They are involved in multiple biological processes such as cell proliferation, migration, invasion, and metastasis by cooperating with different transcription factors, including SIXs (especially SIX1) and c-Myc (11,12). Currently, studies involved in the interaction between SIXs and EYAs in cancer biology have mainly focused on EYA1-SIX1. We have demonstrated that SIX1 and EYA1 are overexpressed in CRC cells and their interactions activate the expression of *CCNA1* and *TGFB1* (10). In the current study, we revealed that SIX5 partners with EYA3 and p300 to transactivate a number of genes, including *EGFR*, *VEGFD*, *MMP3*, *MMP7*, *MMP8*, *MMP21*, and *MMP26*. Of these target genes, *EGFR* is a strong biomarker of multiple cancer types and its OE can promote solid tumor growth (23). The VEGF-mediated signaling is activated in tumor cells, affecting the function of cancer stem cells, angiogenesis, vascular permeability, and the tumor microenvironment (24,25). Meanwhile, MMPs are involved in matrix degradation and remodeling, tumor neovascularization, and metastasis (26). These seven genes have not been previously identified as targets of either EYAs or SIXs, suggesting that we have identified a new group of direct targets of SIX/EYA partners. Besides these seven

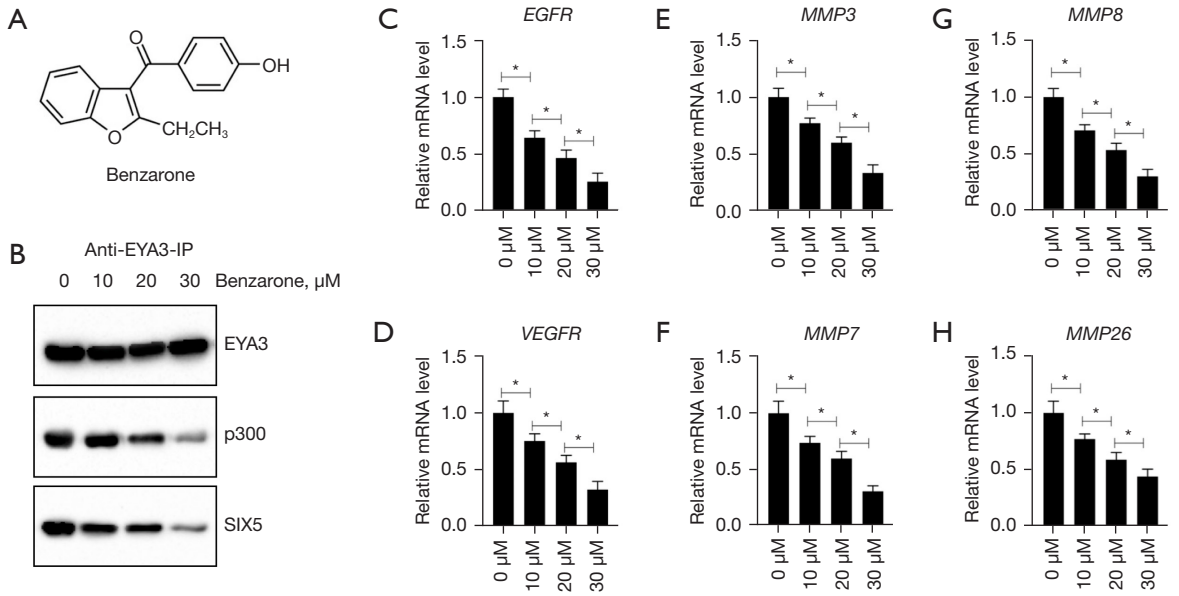

Figure 8 Benzarone attenuated the assembly of the EYA3-p300-SIX5 complex and decreased the expression levels of EYA3-p300-SIX5 target genes. (A) Chemical structure of benzarone. (B) Benzarone attenuated the assembly of the EYA3-SIX5-p300 complex. HCEC-1CT cells were treated with different doses of benzarone (0, 10, 20, and 30 μM), followed by immunoprecipitation with anti-EYA3-conjugated agarose. The outputs were probed using anti-EYA3, anti-p300, and anti-SIX5. (C-H) Benzarone suppressed the expression of EYA3-p300-SIX5 target genes. Cells in (B) were used to measure mRNA levels of *EGFR* (C), *VEGFD* (D), *MMP3* (E), *MMP*7 (F), *MMP8* (G), and *MMP26* (H). *, P<0.05. mRNA, messenger RNA; EGFR, epidermal growth factor receptor; VEGFD, vascular endothelial growth factor receptor; MMP, matrix metalloproteinase.

genes, we also found that some of the 29 dysregulated genes have been reported to participate in tumorigenesis and cancer progression. For instance, cyclin-dependent kinase 3 (*CDK3*) can phosphorylate a subunit of activating protein 1 (AP1) and promote the EMT process in CRC cells (27). Cyclin-dependent kinase inhibitor 1A (*CDKN1A*), also known as *p21*, is a tumor suppressor (28). The suppression of *CDKN1A* in tumor cells mainly affects cell cycle progression, leading to uncontrolled cell proliferation (28). However, the promoters of *CDK3* and *CDKN1A* do not contain the SIX5 binding site, suggesting that they may not be the direct target genes of the EYA3-SIX5-p300 complex.

Dynamic changes of histone acetylation and deacetylation affect chromatin structures, increasing or inhibiting gene expression (29). p300 and its homologue CBP serve as scaffolds to recruit transcription factors and other transcriptional regulators, transactivating gene expression (30). One limitation of this study is that we did not investigate the dynamic changes of p300 substrates by proteomics due to the shortage of experimental technology. We will investigate the effects of dynamic changes of acetylation on the expression levels of *EGFR/VEGFD/MMPs* using p300-specific catalytic inhibitors, bromodomain inhibitors, and p300-knockout cell lines in the future.

Previous publications involved in EYA-SIX-mediated transcription have mainly focused on the interaction between SIXs and EYAs. It is unclear if other transcriptional regulators are involved in the assembly of the EYA-SIX complex. Herein, we discovered that a histone acetyltransferase p300 can be recruited by SIX5, and both EYA3 and p300 are required for the transcription of their target genes. Transcription factors typically recruit p300 to the target gene promoters where p300 acetylates chromatin (31). Although the specific mechanism by which the EYA3-SIX5-p300 complex regulates gene transcription is unclear, we speculate that these three proteins may play their respective roles. One responsibility of SIX5 is binding to its target gene promoters, where it recruits p300 to acetylate chromatin, resulting in the loosened chromatin structure. It further recruits EYA3, which acts as a coactivator to induce the expression of target genes.

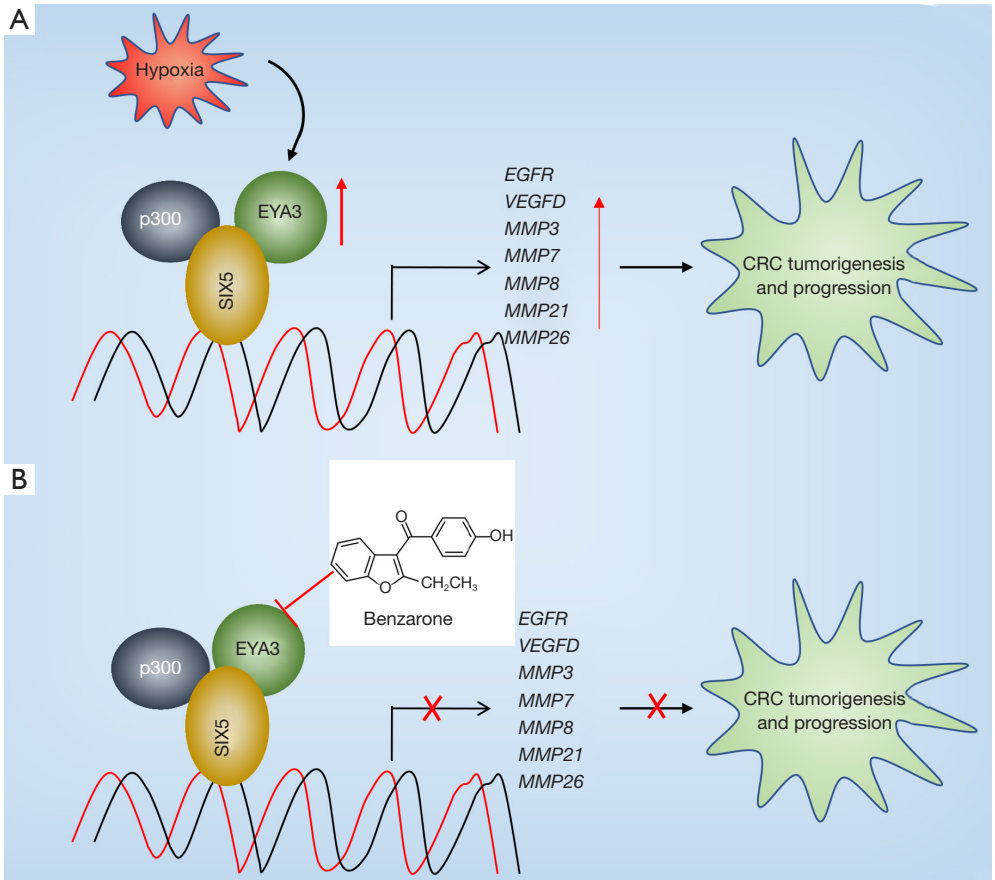

Figure 9 Schematic representation of the EYA3-SIX5-p300 complex in CRC tumorigenesis and cancer progression. (A) Schematic diagram of the EYA3-SIX5-p300 complex in CRC tumorigenesis and cancer progression. Hypoxia induces EYA3, promoting the assembly of the EYA3-SIX5-p300 complex, which binds to the promoters of *EGFR*, *VEGFD*, *MMP3*, *MMP7*, *MMP8*, *MMP21*, and *MMP26*. The induction of these target genes triggers CRC tumorigenesis and promotes cancer progression. (B) Schematic diagram of the disruption of EYA3-SIX5-p300 complex by benzarone. Benzarone impairs the assembly of the EYA3-SIX5-p300 complex, causing the suppression of *EGFR*, *VEGFD*, *MMP3*, *MMP7*, *MMP8*, *MMP21*, and *MMP26*, and attenuating tumor growth. CRC, colorectal cancer; EGFR, epidermal growth factor receptor; VEGFD, vascular endothelial growth factor receptor; MMP, matrix metalloproteinase.

Hypoxia microenvironment is common in solid tumors including CRC because the rapid tumor cell proliferation and abnormal tumor blood vessels outstrip the oxygen supply (32). Hypoxia affects numerous tumor biological processes, such as neovascularization, metabolism, metastasis, apoptosis, autophagy, migration, and chemoresistance (33). Each process is controlled by hypoxia-dependent transcriptional programs involving multiple signaling pathways, such as nuclear factor kappa B (NF-κB), phosphoinositide 3-kinases (PI3Ks), and mitogen-activated protein kinase (MAPK) (32,33). An interesting finding in our study is that hypoxia induces EYA3 and promotes the assembly of the EYA3-SIX5-p300 complex. To our knowledge, this is the first report that EYA3 can be induced by hypoxia. The results that depletion of HIF1α and HIF2α decreases the assembly of EYA3-SIX5-p300 complex suggest that HIF inhibitors may be beneficial to CRC therapy by suppressing *EGFR*, *VEGFD*, *MMP3*, *MMP7*, *MMP8*, *MMP21*, and *MMP26*. However, it is unknown if EYA3 is transcriptionally regulated by the HIF transcription factors. Moreover, *EGFR/VEGFD/MMP* genes are also involved in the transduction of multiple signalings, such as apoptosis, MAPK/PI3K, and NF-κB (34-36). Thus, more efforts are required to explore the crosstalk between hypoxia signaling and other pathways.

In summary, we demonstrated that p300 and the

hypoxia-inducible EYA3 serve as coactivators of SIX5 to transactivate the expression of *EGFR*, *VEGFD*, *MMP3*, *MMP7*, *MMP8*, *MMP21*, and *MMP26*. Inhibition of *EYA3* or specific KD of EYA3-SIX5-p300 members significantly attenuates cell proliferation, invasion, and tumor growth. Our studies uncovered a new mechanism of the assembly of the SIX-associated transcription complex and identified its downstream target genes, providing a new avenue for CRC therapy.

Acknowledgments

Funding: This study was supported by a grant from the National Natural Science Foundation of China (No. 82172909).

Footnote

Reporting Checklist: The authors have completed the ARRIVE reporting checklist. Available at https://atm.amegroups.com/article/view/10.21037/atm-22-2663/rc

Data Sharing Statement: Available at https://atm.amegroups.com/article/view/10.21037/atm-22-2663/dss

Conflicts of Interest: Both authors have completed the ICMJE uniform disclosure form (available at https://atm.amegroups.com/article/view/10.21037/atm-22-2663/coif). The authors have no conflicts of interest to declare.

Ethical Statement: The authors are accountable for all aspects of the work in ensuring that questions related to the accuracy or integrity of any part of the work are appropriately investigated and resolved. Animal experiments were performed under a project license (No. 2018072HA) granted by the ethics board of West China Hospital of Sichuan University, in compliance with guidelines for the care and use of animals at West China Hospital of Sichuan University. The study was conducted in accordance with the Declaration of Helsinki (as revised in 2013).

References

1. Lewandowska A, Rudzki G, Lewandowski T, et al. Title: Risk Factors for the Diagnosis of Colorectal Cancer. Cancer Control 2022;29:10732748211056692.
2. Xi Y, Xu P. Global colorectal cancer burden in 2020 and projections to 2040. Transl Oncol 2021;14:101174.
3. Al-Joufi FA, Setia A, Salem-Bekhit MM, et al. Molecular Pathogenesis of Colorectal Cancer with an Emphasis on Recent Advances in Biomarkers, as Well as Nanotechnology-Based Diagnostic and Therapeutic Approaches. Nanomaterials (Basel) 2022;12:169.
4. Sawicki T, Ruszkowska M, Danielewicz A, et al. A Review of Colorectal Cancer in Terms of Epidemiology, Risk Factors, Development, Symptoms and Diagnosis. Cancers (Basel) 2021;13:2025.
5. Jin Y, Zhang M, Li M, et al. SIX1 Activation Is Involved in Cell Proliferation, Migration, and Anti-inflammation of Acute Ischemia/Reperfusion Injury in Mice. Front Mol Biosci 2021;8:725319.
6. Meurer L, Ferdman L, Belcher B, et al. The SIX Family of Transcription Factors: Common Themes Integrating Developmental and Cancer Biology. Front Cell Dev Biol 2021;9:707854.
7. Blevins MA, Towers CG, Patrick AN, et al. The SIX1-EYA transcriptional complex as a therapeutic target in cancer. Expert Opin Ther Targets 2015;19:213-25.
8. Coletta RD, Christensen KL, Micalizzi DS, et al. Six1 overexpression in mammary cells induces genomic instability and is sufficient for malignant transformation. Cancer Res 2008;68:2204-13.
9. Behbakht K, Qamar L, Aldridge CS, et al. Six1 overexpression in ovarian carcinoma causes resistance to TRAIL-mediated apoptosis and is associated with poor survival. Cancer Res 2007;67:3036-42.
10. Wu J, Huang B, He HB, et al. Two naturally derived small molecules disrupt the sineoculis homeobox homolog 1-eyes absent homolog 1 (SIX1-EYA1) interaction to inhibit colorectal cancer cell growth. Chin Med J (Engl) 2021;134:2340-52.
11. Zhang L, Zhou H, Li X, et al. Eya3 partners with PP2A to induce c-Myc stabilization and tumor progression. Nat Commun 2018;9:1047.
12. Vartuli RL, Zhou H, Zhang L, et al. Eya3 promotes breast

tumor-associated immune suppression via threonine phosphatase-mediated PD-L1 upregulation. J Clin Invest 2018;128:2535-50.
13. Coletta RD, Christensen K, Reichenberger KJ, et al. The Six1 homeoprotein stimulates tumorigenesis by reactivation of cyclin A1. Proc Natl Acad Sci U S A 2004;101:6478-83.
14. Xu J, Li J, Zhang T, et al. Chromatin remodelers and lineage-specific factors interact to target enhancers to establish proneurosensory fate within otic ectoderm. Proc Natl Acad Sci U S A 2021;118:e2025196118.
15. Eisner A, Pazyra-Murphy MF, Durresi E, et al. The Eya1 phosphatase promotes Shh signaling during hindbrain development and oncogenesis. Dev Cell 2015;33:22-35.
16. Wang CA, Jedlicka P, Patrick AN, et al. SIX1 induces lymphangiogenesis and metastasis via upregulation of VEGF-C in mouse models of breast cancer. J Clin Invest 2012;122:1895-906.
17. Cheng Q, Ning D, Chen J, et al. SIX1 and DACH1 influence the proliferation and apoptosis of hepatocellular carcinoma through regulating p53. Cancer Biol Ther 2018;19:381-90.
18. Chen H, Pugh BF. What do Transcription Factors Interact With? J Mol Biol 2021;433:166883.
19. Samuels DS, Lybecker MC, Yang XF, et al. Gene Regulation and Transcriptomics. Curr Issues Mol Biol 2021;42:223-66.
20. Chen Z. The transrepression and transactivation roles of CtBPs in the pathogenesis of different diseases. J Mol Med (Berl) 2021;99:1335-47.
21. Abou Khouzam R, Brodaczewska K, Filipiak A, et al. Tumor Hypoxia Regulates Immune Escape/Invasion: Influence on Angiogenesis and Potential Impact of Hypoxic Biomarkers on Cancer Therapies. Front Immunol 2020;11:613114.
22. Zhou H, Blevins MA, Hsu JY, et al. Identification of a Small-Molecule Inhibitor That Disrupts the SIX1/EYA2 Complex, EMT, and Metastasis. Cancer Res 2020;80:2689-702.
23. Lawal B, Wang YC, Wu ATH, et al. Pro-Oncogenic c-Met/EGFR, Biomarker Signatures of the Tumor Microenvironment are Clinical and Therapy Response Prognosticators in Colorectal Cancer, and Therapeutic Targets of 3-Phenyl-2H-benzoe1,3-Oxazine-2,4(3H)-Dione Derivatives. Front Pharmacol 2021;12:691234.
24. Dakowicz D, Zajkowska M, Mroczko B. Relationship between VEGF Family Members, Their Receptors and Cell Death in the Neoplastic Transformation of Colorectal Cancer. Int J Mol Sci 2022;23:3375.
25. Ilson DH. Emerging evidence for VEGF and immune checkpoint inhibition in oesophagogastric cancer. Lancet Gastroenterol Hepatol 2022;7:200-1.
26. Cheng T, Chen P, Chen J, et al. Landscape Analysis of Matrix Metalloproteinases Unveils Key Prognostic Markers for Patients With Breast Cancer. Front Genet 2021;12:809600.
27. Zheng D, Cho YY, Lau AT, et al. Cyclin-dependent kinase 3-mediated activating transcription factor 1 phosphorylation enhances cell transformation. Cancer Res 2008;68:7650-60.
28. Lossaint G, Horvat A, Gire V, et al. Reciprocal regulation of p21 and Chk1 controls the cyclin D1-RB pathway to mediate senescence onset after G2 arrest. J Cell Sci 2022;135:jcs259114.
29. Bannister AJ, Kouzarides T. Regulation of chromatin by histone modifications. Cell Res 2011;21:381-95.
30. Weinert BT, Narita T, Satpathy S, et al. Time-Resolved Analysis Reveals Rapid Dynamics and Broad Scope of the CBP/p300 Acetylome. Cell 2018;174:231-244.e12.
31. Maldotti M, Lauria A, Anselmi F, et al. The acetyltransferase p300 is recruited in trans to multiple enhancer sites by lncSmad7. Nucleic Acids Res 2022;50:2587-602.
32. Wigerup C, Påhlman S, Bexell D. Therapeutic targeting of hypoxia and hypoxia-inducible factors in cancer. Pharmacol Ther 2016;164:152-69.
33. Muz B, de la Puente P, Azab F, et al. The role of hypoxia in cancer progression, angiogenesis, metastasis, and resistance to therapy. Hypoxia (Auckl) 2015;3:83-92.
34. Mamo M, Ye IC, DiGiacomo JW, et al. Hypoxia Alters the Response to Anti-EGFR Therapy by Regulating EGFR Expression and Downstream Signaling in a DNA Methylation-Specific and HIF-Dependent Manner. Cancer Res 2020;80:4998-5010.
35. Goel HL, Mercurio AM. VEGF targets the tumour cell. Nat Rev Cancer 2013;13:871-82.
36. Quintero-Fabián S, Arreola R, Becerril-Villanueva E, et al. Role of Matrix Metalloproteinases in Angiogenesis and Cancer. Front Oncol 2019;9:1370.

Cite this article as: Yang C, Liu H. Both a hypoxia-inducible EYA3 and a histone acetyltransferase p300 function as coactivators of SIX5 to mediate tumorigenesis and cancer progression. Ann Transl Med 2022;10(13):752. doi: 10.21037/atm-22-2663

Supplementary

Table S1 Vectors, insertion sites, and primer sequences

Vectors	Enzyme sites	Forward primers	Reverse primers
pCDNA3-Flag-EYA3	BamHI + XhoI	CGGGATCCATGGAAGAAGAGCAAGATTTAC	CCGCTCGAGTTAGAGAAAATCAAGCTCTAAAGCCT
pCDNA3-Myc-EYA3	KpnI + XhoI	GGGGTACCATGGAAGAAGAGCAAGATTTAC	CCGCTCGAGTTAGAGAAAATCAAGCTCTAAAGCCT
pCDNA3-Myc-p300	KpnI + XhoI	GGGGTACCATGGCCGAGAATGTGGTGGAACCG	CCGCTCGAGCTAGTGTATGTCTAGTGTACTCTG
pCDNA3-Myc-SIX5	KpnI + XhoI	GGGGTACCATGGCTACCTTGCCTGCGGAG	CCGCTCGAGTCACAGTTCCAAGGGCTCCTCCA
pCDNA3-Flag-p300	BamHI + XhoI	CGGGATCCATGGCCGAGAATGTGGTGGAACCG	CCGCTCGAGCTAGTGTATGTCTAGTGTACTCTG

Table S2 shRNA information (ordered from Sigma-Aldrich)

Genes	shRNA target sequences	Catalog numbers
EYA3	CCCTTCTACAAGTCCATCTTT	TRCN0000051603
	CACATTATTCTTATCCCATT	TRCN0000051606
SIX5	GCGCCAGCTCTTGCAGACTTT	TRCN0000015773
	CCCTGCCAATGTGCACCTCAT	TRCN0000015775
p300	CAATTCCGAGACATCTTGAGA	TRCN0000009883
	GCCTTCACAATTCCGAGACAT	TRCN0000039885
HIF1α	CCGCTGGAGACACAATCATAT	TRCN0000003808
	TGCTCTTTGTGGTTGGATCTA	TRCN0000010819
HIF2α	AGGTGGAGCTAACAGGACATA	TRCN0000003803
	CAGTACCCAGACGGATTTCAA	TRCN0000003806

shRNA, short hairpin RNA.

https://dx.doi.org/10.21037/atm-22-2663

Table S3 Primers used for RT-qPCR analysis to measure gene expression

Genes	Forward primers	Reverse primers
EYA3	GAGGCAAGACTCCTTCCAATGC	GAGCACTGACTTCAGCTACTCAG
HIF1α	TACTGCTAATGCCACCACTACCA	TGGTGATGATGTGGCACTAGTAG
HIF2α	AGACTTGTCCAGTGCTCCCACG	GCTGAATGACTCCACTGCTCGGAT
SIX5	TGCCAATGTGCACCTCATCAACTC	ATGGGGCTGCCAGACACAGGGTTG
p300	TGGCTTAGATGATGAGAGCAACA	ATTCCGACACTGGCAAGCATGGA
EGFR	AGCGTTCAATTCATCCTCACCAG	CTCACAAAGGAGGGAAGAGACTGG
VEGFD	GATGTTGTACGTCCAGCTGGT	CCAAACTAGAAGCAGCCCTGAT
MMP3	GAGGTGACTCCACTCACATTC	GGCATAGGCATGGGCCAAAACAT
MMP7	GTGGTCACCTACAGGATCGTATC	AGCAGTTCCCCATACAACTTTCC
MMP8	ATGAATGTGAGCTTACCAGGGT	CCTAGGTGACTATGCCTCTCTTC
MMP13	ATCCAGTCTCTCTATGGTCCAG	TCATTGTTTCTCCTCGGAGACT
MMP21	ACAATAGGACACGCTATGGGGA	GTCACTGTCATATCTCCAGTA
MMP26	GACATGCAGATGCATGCTCTGCT	CCTGTAAGTTAGAGTGTGC
RNF5	ATGTCTTCATCAGTGGCTGGA	TTAATCTGGGATCCTGGGGCT
TAP2	TGAACACTGCTACCTGCACAG	CATCACCTTATCATCTTCGCAG
STMN1	ATCCAAAGACTGTACTGGCCAG	CAGTTTCTCCCCTTTAGCCCCTA
BRD2	AGCTGCAATACCTACACAAGGT	AGTACCCATGTCCATAGGCTG
b-Actin	CACCATTGGCAATGAGCGGTTC	AGGTCTTTGCGGATGTCCACGT

RT-qPCR, real-time quantitative polymerase chain reaction.

Table S4 Primers used for ChIP RT-qPCR analysis

Genes	Forward primers	Reverse primers
EGFR	TACTGCAGGAGAAGGAACAGT	GTCCCACTGCCCCTGTAGCT
VEGFD	TGAACATTTGAGTCAGTTCTTA	GCACAACCTTCATGGAAGCTTG
MMP3	ATGTTCTATTCTGCCCATGAG	CTATATACAATTATACTC
MMP7	CGCATCACCATGTTTGGCTA	ATGCAAAGACACATCCATGG
MMP8	ACAAAGAATGGGTTGCTACA	ACAGCAGTGGTGTGGAGGGAGT
MMP13	TACCTCTGTCTGAATCTGT	TGGAGGTGCTACGGCACAAC
MMP21	CCGCAGTATATCTCCATAG	TGGTGTGAGAACTCCTTCTC
MMP26	ACTCTGGCTCTATGCAAAGTT	GTCTATCTTCACTCTTTCTTCCC

ChIP, chromatin immunoprecipitation; RT-qPCR, real-time quantitative polymerase chain reaction.

https://dx.doi.org/10.21037/atm-22-2663

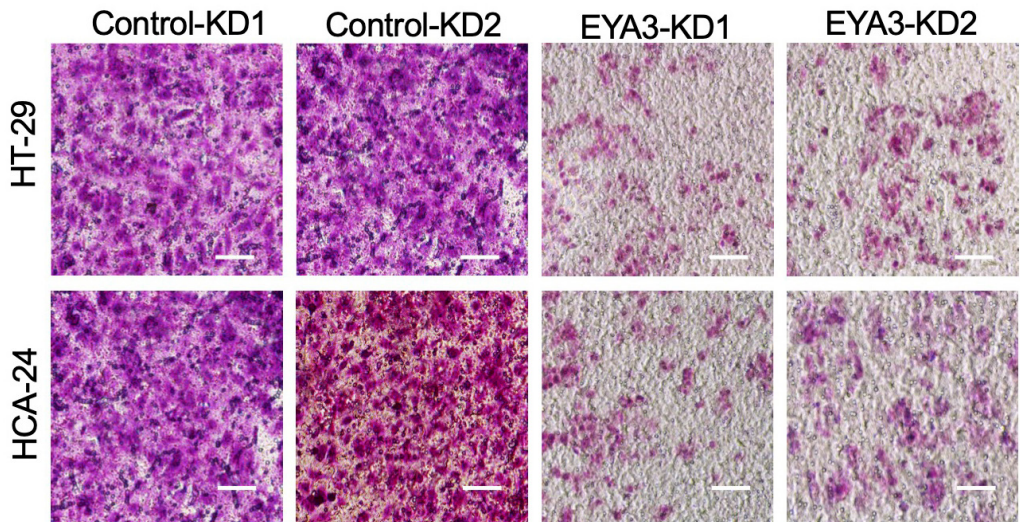

Figure S1 Cell invasion assay using control-KD and EYA3-KD cells. The same numbers of control-KD and EYA3-KD cells under both HT-29 and HCA-24 backgrounds were seeded into the upper chamber of Boyden chambers. After culturing for 24 h, the invaded cells in the lower chambers were fixed in methanol and stained with 0.2% crystal violet. Cells were photographed using a microscope with the magnification of 20-fold. Bars =100 μm. KD, knockdown.

https://dx.doi.org/10.21037/atm-22-2663

Table S5 EYA3-interacting proteins by MS analysis

Proteins	Protein description	Percolator score	Molecular weight (kD)	Matched queries	Matched peptides
EYA3	Eyes Absent Homolog 3	7123	63	57	43
SIX5	Sine Oculis Homeobox Homolog 5	6877	75	35	27
HMGN2	High Mobility Group Nucleosomal Binding Domain 2	6536	9	11	9
WDR1	WD Repeat Domain 1	6233	66	18	6
TRNP1	TMF1 Regulated Nuclear Protein 1	6094	23	8	5
MAPK8	Mitogen-Activated Protein Kinase 8	5887	48	20	10
p300	Histone Acetyltransferase P300	5649	264	33	18
KPNA2	Karyopherin Subunit Alpha 2	5369	58	32	11
TDP1	Tyrosyl-DNA Phosphodiesterase 1	5332	68	26	14
MDC1	Mediator Of DNA Damage Checkpoint 1	5128	227	44	27
UIMC1	Ubiquitin Interaction Motif Containing 1	4890	80	36	29
SMAD4	Mothers Against Decapentaplegic Homolog 4	4776	60	42	20
PITX1	Paired Like Homeodomain 1	4654	34	15	11
STIP1	Stress Induced Phosphoprotein 1	4454	63	25	12
CRY1	Cryptochrome Circadian Regulator 1	4092	66	30	25
MTMR3	Myotubularin Related Protein 3	3854	134	44	31
DLX2	Distal-Less Homeobox 2	3667	34	21	10
CHD9	Chromodomain Helicase DNA Binding Protein 9	3452	326	33	24
DIDO1	Death Inducer-Obliterator 1	3255	244	35	18
DDB2	Damage Specific DNA Binding Protein 2	3095	48	20	17
CDK1	Cyclin Dependent Kinase 1	3011	34	17	11
OGG1	8-Oxoguanine DNA Glycosylase	2943	39	18	10
COPS5	COP9 Signalosome Subunit 5	2901	38	24	20
RPA3	Replication Protein A3	2883	14	10	5
DNA2	DNA Replication Helicase/Nuclease 2	2654	120	25	17
HUS1	HUS1 Checkpoint Clamp Component	2412	32	16	10
GPS1	G Protein Pathway Suppressor 1	2267	56	25	21
RMI1	RecQ Mediated Genome Instability 1	2198	70	33	13
POLD4	DNA Polymerase Delta 4	2006	12	9	8
MCRS1	Microspherule Protein 1	1966	52	19	10
MCPH1	Microcephalin 1	1934	93	24	17
BAG6	BAG Cochaperone 6	1835	119	27	22
MYOD1	Myogenic Differentiation 1	1802	35	17	10
CNTN2	Contactin 2	1771	113	33	29
IRF3	Interferon Regulatory Factor 3	1643	47	27	20
HIPK2	Homeodomain Interacting Protein Kinase 2	1512	131	44	25
PTGS2	Prostaglandin-Endoperoxide Synthase 2	1442	69	33	27
SKP2	S-Phase Kinase Associated Protein 2	1023	48	19	10
BRD4	Bromodomain Containing 4	1009	152	44	18
NAP1L1	Nucleosome Assembly Protein 1 Like 1	954	45	24	11
NPM1	Nucleophosmin 1	903	33	15	10
DDX5	DEAD-Box Helicase 5	884	69	26	18
FEN1	Flap Structure-Specific Endonuclease 1	825	43	17	11
PIN1	Peptidylprolyl Cis/Trans Isomerase, NIMA-Interacting 1	775	18	10	7
NRG1	Neuregulin 1	701	70	32	23
NUDT21	Nudix Hydrolase 21	665	26	22	11
NOS2	Nitric Oxide Synthase 2	632	131	42	32
USP1	Ubiquitin Specific Peptidase 1	607	88	34	27
DUX4	Double Homeobox 4	587	45	25	20
IPO7	Importin 7	543	120	44	19
PLK1	Polo Like Kinase 1	513	68	35	22
DCAF7	DDB1 And CUL4 Associated Factor 7	486	39	20	19
SSRP1	Structure Specific Recognition Protein 1	447	81	34	20
CBX1	Chromobox 1	406	21	18	6
EEF2	Eukaryotic Translation Elongation Factor 2	367	95	17	8
SNTB2	Syntrophin Beta 2	332	58	15	4
RBM25	RNA Binding Motif Protein 25	302	100	25	7
CCN2	Cellular Communication Network Factor 2	285	38	21	17
CDR2	Cerebellar Degeneration Related Protein 2	265	52	16	10
CTNND2	Catenin Delta 2	234	133	22	11
HK2	Hexokinase 2	226	102	16	9
DDX1	DEAD-Box Helicase 1	213	82	25	19

MS, mass spectrometry.

https://dx.doi.org/10.21037/atm-22-2663

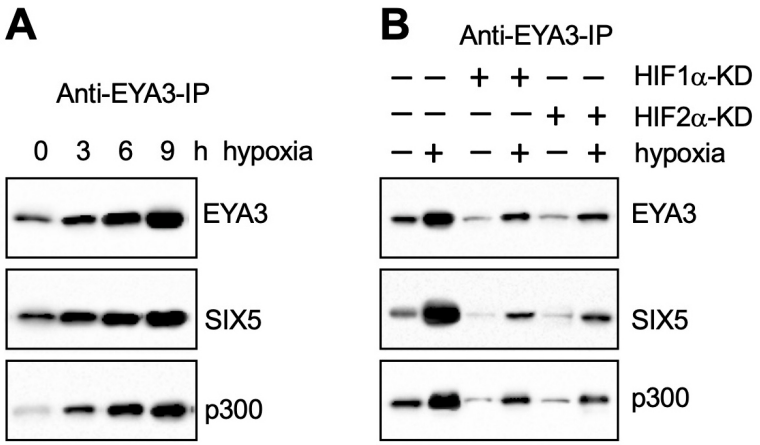

Figure S2 Hypoxia promoted the assembly of EYA3-SIX5-p300 complex. (A) The effect of hypoxia on the assembly of EYA3-SIX5-p300 complex. HCEC-1CT cells were treated with hypoxia for 0, 3, 6, and 9 h, followed by immunoprecipitation with anti-EYA3-conjugated agarose. The outputs were probed using anti-EYA3, anti-SIX5, and anti-p300. (B) The effect of HIF1α/2α depletion on the assembly of EYA3-SIX5-p300 complex. The Control-KD, HIF1α-KD1, and HIF2α-KD1 cells were treated with or without hypoxia for 9 h, followed by immunoprecipitation with anti-EYA3-conjugated agarose. The outputs were probed using anti-EYA3, anti-SIX5, and anti-p300.

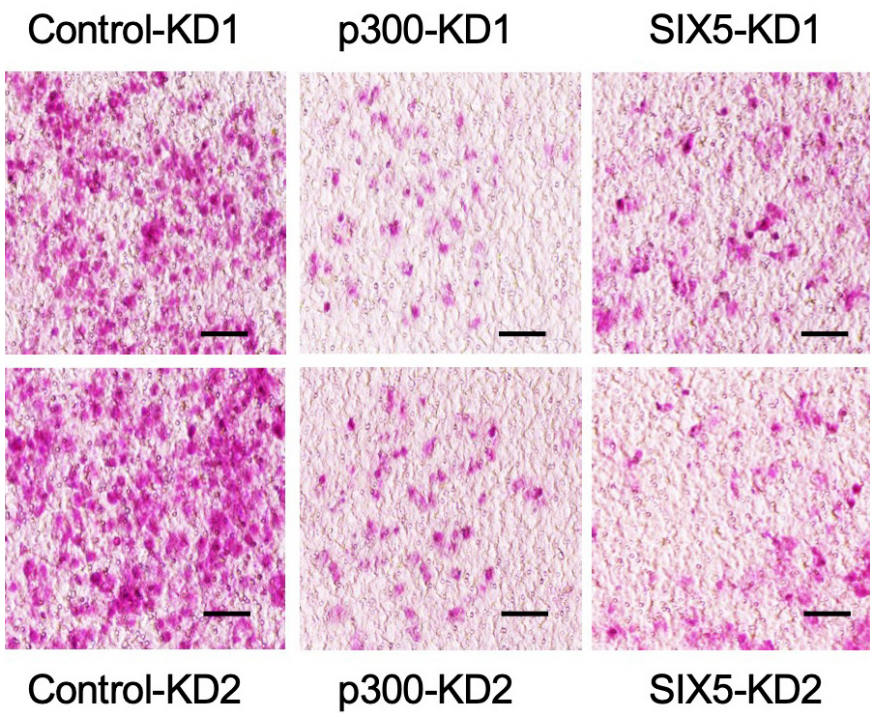

Figure S3 Cell invasion assay using control-KD, p300-KD, and SIX5-KD cells. The same numbers of control-KD, p300-KD, and SIX5-KD cells under HT-29 background were seeded into the upper chamber of Boyden chambers. After culturing for 24 h, the invaded cells in the lower chambers were fixed in methanol and stained with 0.2% crystal violet. Cells were photographed using a microscope with the magnification of 20-fold. Bars =100 μm. KD, knockdown.

https://dx.doi.org/10.21037/atm-22-2663

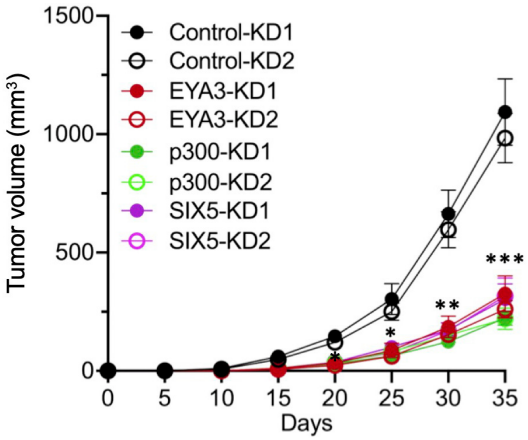

Figure S4 Tumor volumes in mice administrated with control-KD, EYA3-KD, p300-KD, and SIX5-KD cells. The control-KD, EYA3-KD, p300-KD, and SIX5-KD cells were injected into nude mice (n=10 for each cell line). Tumor volumes were determined at 5-day intervals. * P<0.05, ** P<0.01, and *** P<0.001.

https://dx.doi.org/10.21037/atm-22-2663

Table S6 Differentially expressed genes by microarray analysis

Genes	Gene description	Control-KD1	EYA3–KD1	p300–KD1
EGFR	Epidermal Growth Factor Receptor	2	–12.1	–11.4
VEGFD	Vascular Endothelial Growth Factor D	2	–9.4	–8.5
MMP8	Matrix Metallopeptidase 8	2	–10.2	–9.6
MMP3	Matrix Metallopeptidase 3	2	–8.6	–8.9
MMP7	Matrix Metallopeptidase 7	2	–8.1	–10.3
MMP26	Matrix Metallopeptidase 26	2	–6.7	–8.5
MMP21	Matrix Metallopeptidase 21	2	–6.5	–6.8
LEMD2	LEM Domain Nuclear Envelope Protein 2	2	–5.7	–7.4
HCG25	HLA Complex Group 25	2	–5.2	–6.7
DDX58	DExD/H-Box Helicase 58	2	–4.6	–5.8
CDK3	Cyclin Dependent Kinase 3	2	–4.2	–6.2
HMGN4	High Mobility Group Nucleosomal Binding Domain 4	2	–4	–5.5
GPN2	GPN-Loop GTPase 2	2	–3.5	–3.7
HOXB2	Homeobox B2	2	–3.2	–3.1
MXD1	MAX Dimerization Protein 1	2	–2.2	–3.4
NUP85	Nucleoporin 85	2	–2.2	–3.1
NFX1	Nuclear Transcription Factor, X-Box Binding 1	2	13.2	11.1
STMN1	Stathmin 1	2	10.9	11.9
BRD2	Bromodomain Containing 2	2	9.9	10.6
GBP2	Guanylate Binding Protein 2	2	9.4	8.7
NOP56	NOP56 Ribonucleoprotein	2	9.1	8.2
CDKN1A	Cyclin Dependent Kinase Inhibitor 1A	2	8.4	9.4
MYOD1	Myogenic Differentiation 1	2	8.2	6.7
TDP1	Tyrosyl-DNA Phosphodiesterase 1	2	7.5	7.2
BRCC3	BRCA1/BRCA2-Containing Complex Subunit 3	2	7	5.4
MDC1	Mediator Of DNA Damage Checkpoint 1	2	6.5	7.8
TBK1	TANK Binding Kinase 1	2	6.2	4.3
CHD7	Chromodomain Helicase DNA Binding Protein 7	2	5.4	5.6
DLX3	Distal-Less Homeobox 3	2	4.3	3.4

https://dx.doi.org/10.21037/atm-22-2663

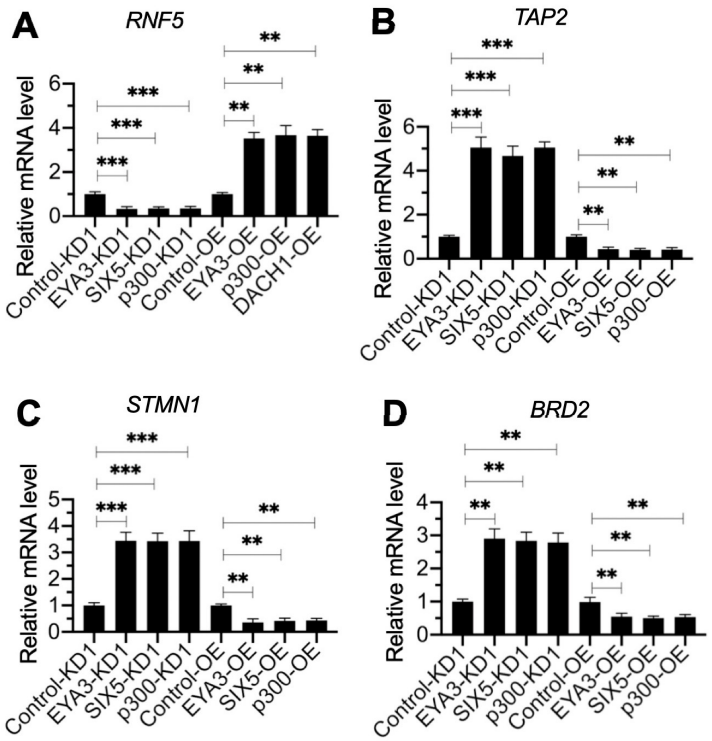

Figure S5 The mRNA levels of RNF5, TAP2, STMN1, and BRD2 in the KD and OE cell lines of EYA3-p300-SIX5 members. The mRNA levels of *RNF5* (A), *TAP2* (B), *STMN1* (C), and *BRD2* (D) in the KD and OE cell lines of EYA3, p300, and SIX5. ** P<0.01, and *** P<0.001. mRNA, messenger RNA; KD, knockdown; OE, overexpression.

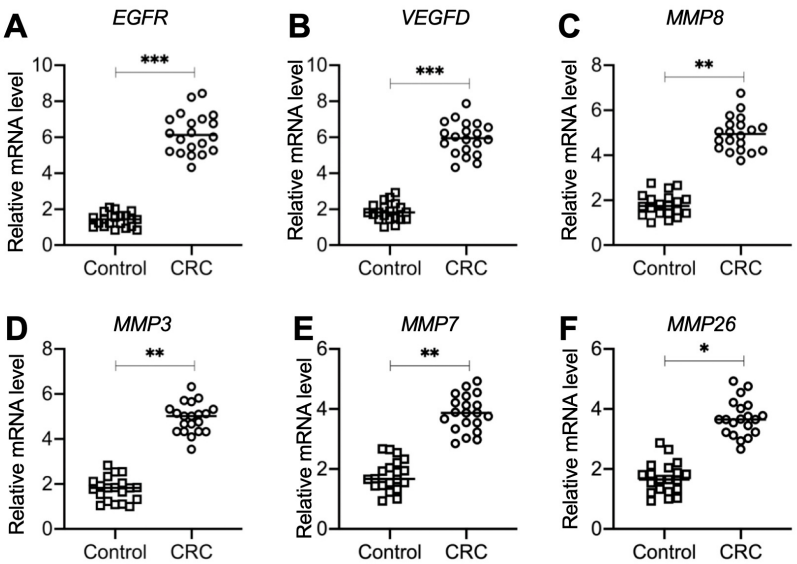

Figure S6 The mRNA levels of EYA3-p300-SIX5 targets in CRC biopsies. The same RNA samples as in Figure 1A were used for qRT-PCR analyses to measure mRNA levels of *EGFR* (A), *VEGFD* (B), *MMP8* (C), *MMP3* (D), *MMP7* (E), and *MMP26* (F). * P<0.05, ** P<0.01, and *** P<0.001. mRNA, messenger RNA; qRT-PCR, quantitative real-time polymerase chain reaction; EGFR, epidermal growth factor receptor; VEGFD, vascular endothelial growth factor receptor; MMP, matrix metalloproteinase.

https://dx.doi.org/10.21037/atm-22-2663

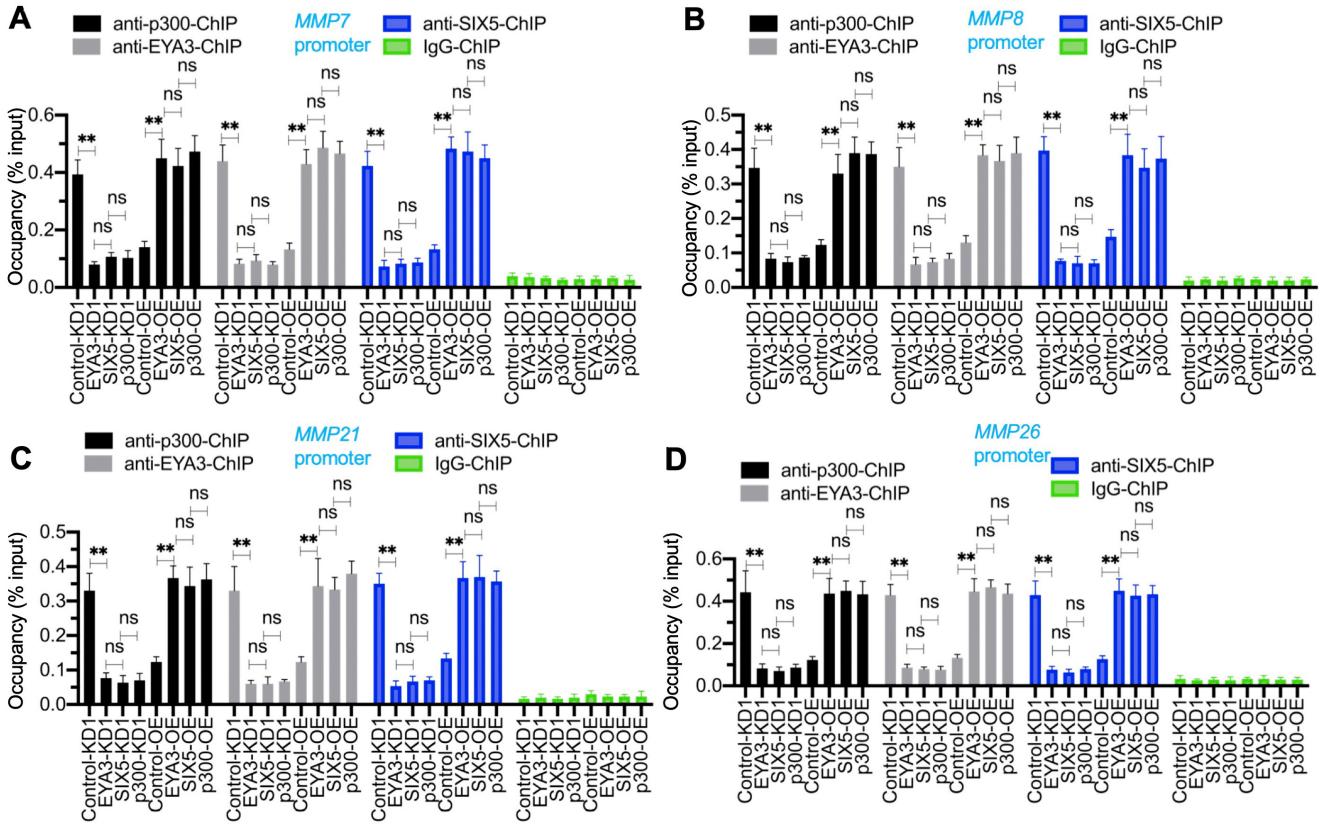

Figure S7 The EYA3-p300-SIX5 members bound to the promoters of MMP7, MMP8, MMP21, and MMP26. The same input and output DNA as used in Figure 6B were subjected to qRT-PCR analyses to measure the enrichment of EYA3-p300-SIX5 members on the promoters of *MMP7* (A), *MMP8* (B), *MMP21* (C), and *MMP26* (D). ns: no significant difference; ** P<0.01. qRT-PCR, quantitative real-time polymerase chain reaction; MMP, matrix metalloproteinase.

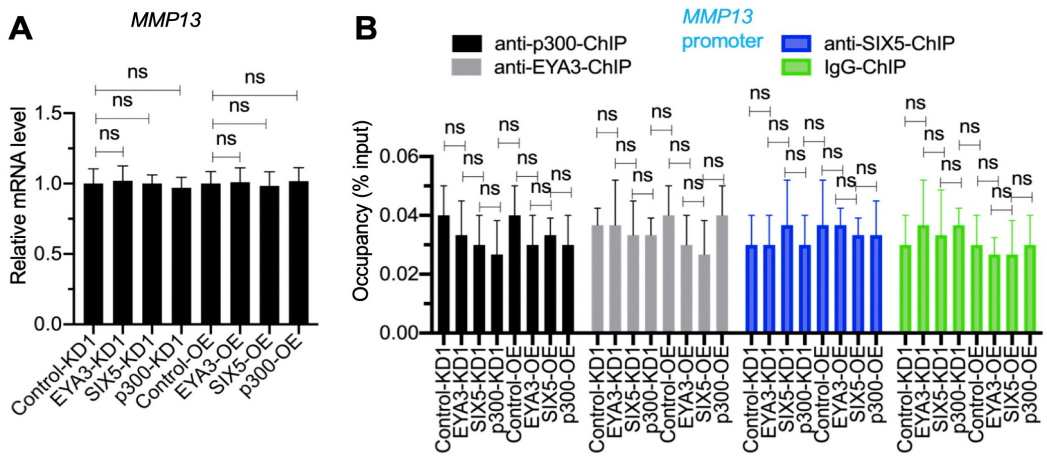

Figure S8 MMP13 was not a target of EYA3-p300-SIX5 complex. (A) *MMP13* mRNA levels in the KD and OE cell lines of EYA3-p300-SIX5 members. ns: no significant difference. (B) ChIP results. The same input and output DNA as used in *Figure 6B* were subjected to qRT-PCR analyses to measure the enrichment of EYA3-p300-SIX5 members on the promoters of *MMP13*. ns, no significant difference; MMP, matrix metalloproteinase; KD, knockdown; OE, overexpression; qRT-PCR, quantitative real-time polymerase chain reaction.

https://dx.doi.org/10.21037/atm-22-2663

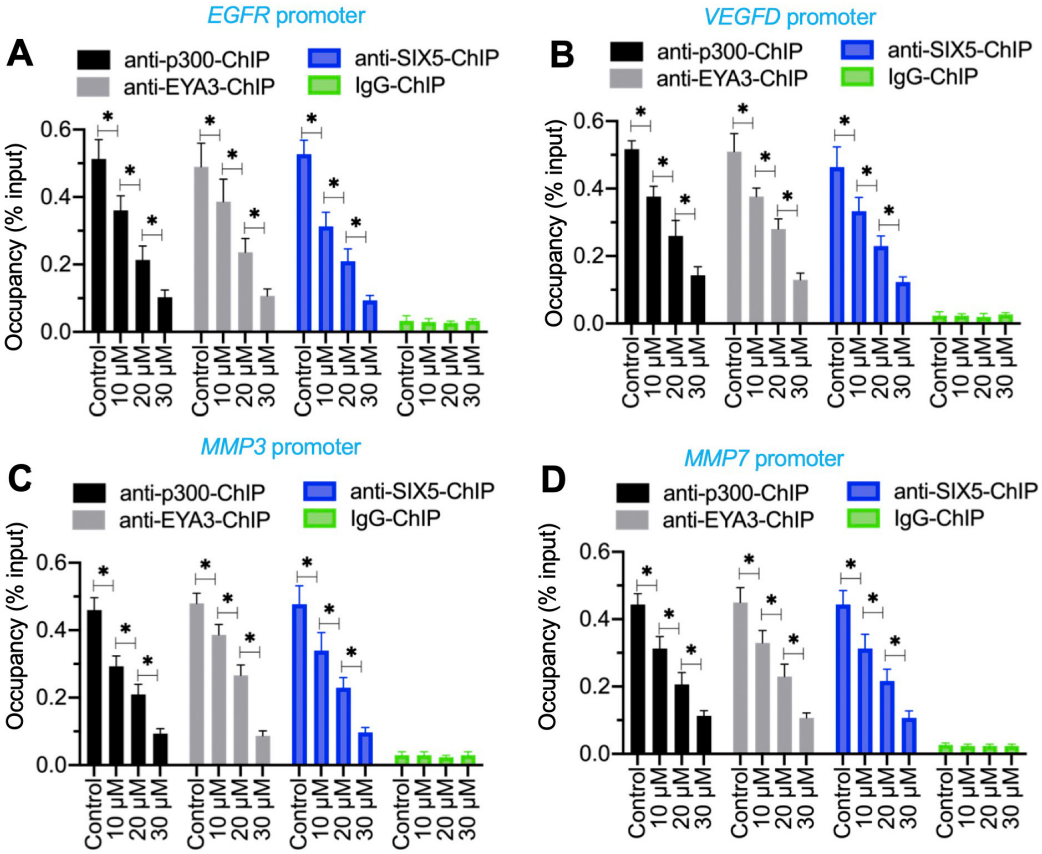

Figure S9 Benzarone attenuated the occupancies of EYA3-p300-SIX5 components on the promoters of *EGFR*, *VEGFD*, *MMP3*, *and MMP7*. HCEC-1CT cells were treated with different doses of benzarone (0, 10, 20, and 30 μM) for 12 h, followed by ChIP assays using anti-p300, anti-EYA3, anti-SIX5, and IgG (negative control). The input and output DNA were subjected to qRT-PCR analyses to measure the enrichment of EYA3-p300-SIX5 components on the promoters of *EGFR* (A), *VEGFD* (B), *MMP3* (C), and *MMP7* (D). * P<0.05. EGFR, epidermal growth factor receptor; VEGFD, vascular endothelial growth factor receptor; MMP, matrix metalloproteinase; ChIP, chromatin immunoprecipitation; qRT-PCR, quantitative real-time polymerase chain reaction.

https://dx.doi.org/10.21037/atm-22-2663

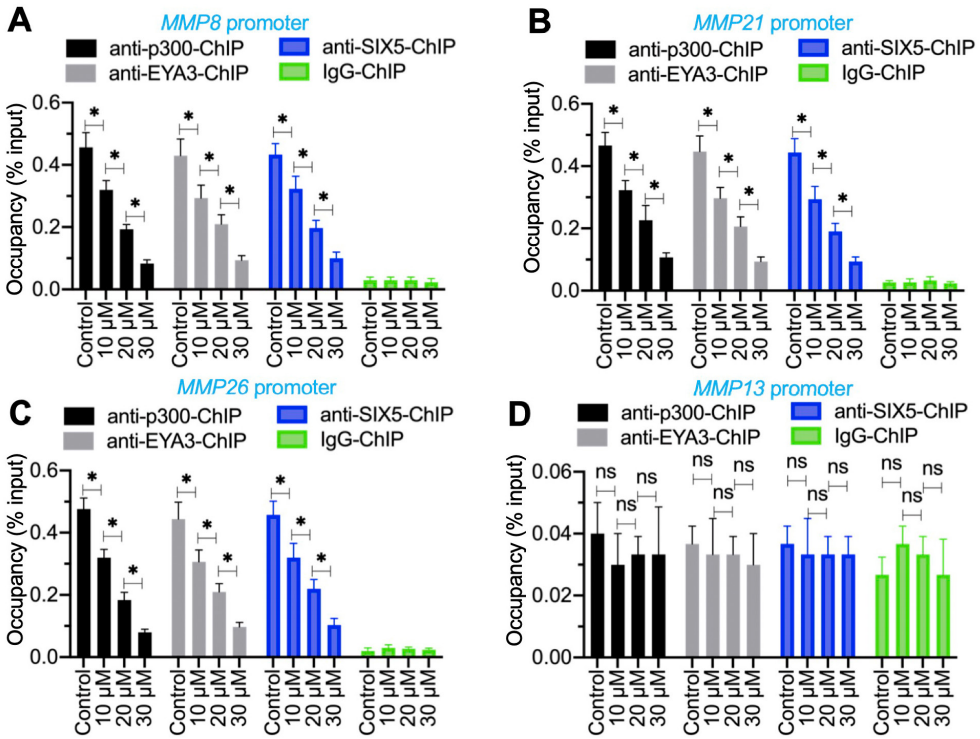

Figure S10 Benzarone attenuated the occupancies of EYA3-p300-SIX5 components on the promoters of *MMP8*, *MMP21*, *MMP26*, and *MMP13*. The same input and output DNA as used in Figure S9 were subjected to qRT-PCR analyses to measure the enrichment of EYA3-p300-SIX5 components on the promoters of *MMP8* (A), *MMP21* (B), *MMP26* (C), and *MMP13* (D). * P<0.05. ns, no significant difference; MMP, matrix metalloproteinase; qRT-PCR, quantitative real-time polymerase chain reaction.

https://dx.doi.org/10.21037/atm-22-2663

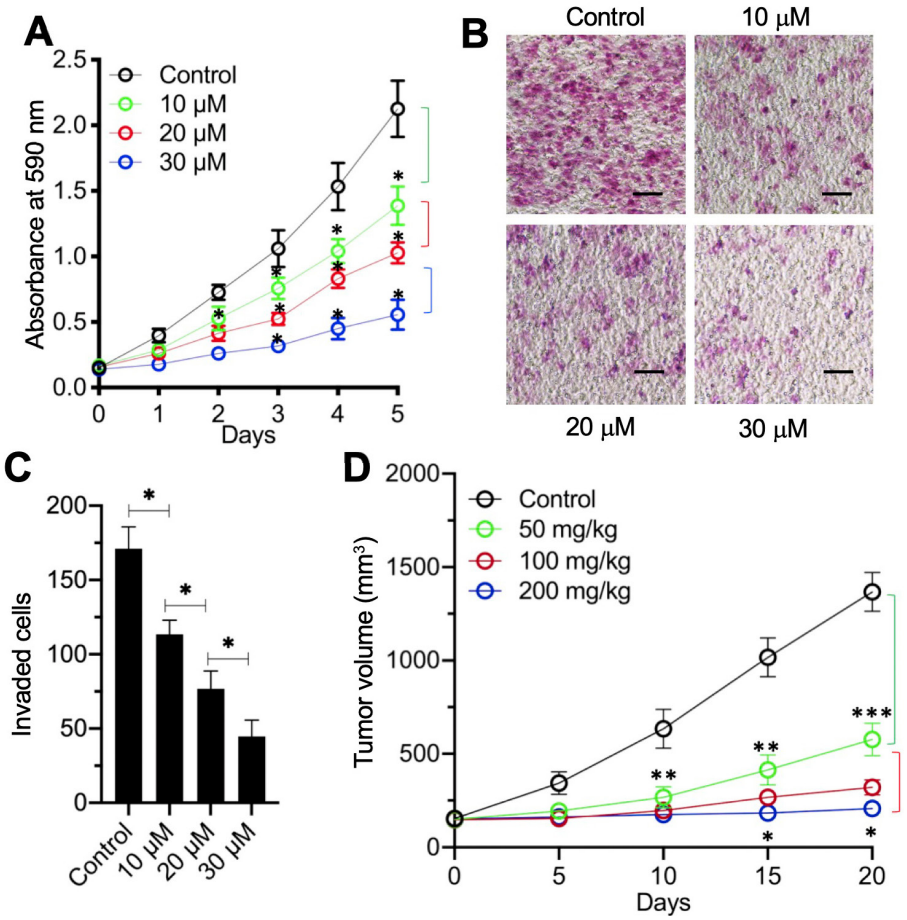

Figure S11 Benzarone inhibited cell proliferation, invasion, and tumor growth. (A) Cell viability in benzarone-treated HT-29 cells (0, 10, 20, and 30 μM) at different time points (days 0, 1, 2, 3, 4, and 5). * P<0.05. (B,C) Cell invasion results. The benzarone-treated HT-29 cells (0, 10, 20, and 30 μM) were seeded into the upper chamber of Boyden chambers. After culturing for 24 h, the invaded cells in the lower chambers were fixed in methanol and stained with 0.2% crystal violet. Cells were photographed using a microscope with the magnification of 20-fold. Bars =100 μm (B). (C) Quantified cell numbers in (B). * P<0.05. (D) Tumor volumes. HT-29 cells were injected into nude mice to generate tumors. After tumor volumes reached approximately 150 mm^3, mice were randomly grouped and administrated with PBS (Control) and different doses of benzarone (50, 100, and 200 mg/kg) at 5-day intervals (n=10 for each concentration). Tumor volumes were determined at 5-day intervals. * P<0.05, ** P<0.01, ***, P<0.001. PBS, phosphate-buffered saline.

https://dx.doi.org/10.21037/atm-22-2663